Telomerase RNA component knockout exacerbates *S. aureus* pneumonia by extensive inflammation and dysfunction of T cells

Yasmina Reisser[1], Franziska Hornung[1], Antje Häder[1], Thurid Lauf[1,2], Sandor Nietzsche[3], Bettina Löffler[1], Stefanie Deinhardt-Emmer[1*]

[1] Institute of Medical Microbiology, Jena University Hospital, Am Klinikum 1, 07747 Jena, Germany

[2] Else Kröner Graduate School for Medical Students "JSAM", Jena University Hospital, 07747 Jena, Germany

[3] Center for Electron Microscopy, Jena University Hospital, Ziegelmühlenweg 1, 07743 Jena, Germany

Correspondence

* Stefanie Deinhardt-Emmer (stefanie.deinhardt-emmer@med.uni-jena.de) and Yasmina Reisser (yasmina.reisser@med.uni-jena.de)

ORCID

SDE 0000-0003-4495-4052

FH 0000-0002-9942-5572

AH 0000-0001-8496-1754

YR 0009-0007-9757-5036

Keywords: *Staphylococcus aureus*, pneumonia, aging, Terc, T cells, inflammation, macrophages

Abstract

The telomerase RNA component (Terc) constitutes a non-coding RNA critical for telomerase function, commonly associated with aging and pivotal in immunomodulation during inflammation.

Our study unveils heightened susceptibility to pneumonia caused by *Staphylococcus aureus (S. aureus)* in *Terc* knockout ($Terc^{ko/ko}$) mice compared to both young and old infected counterparts. The exacerbated infection in $Terc^{ko/ko}$ mice correlates with heightened inflammation, manifested by elevated interleukin-1β (IL-1β) levels and activation of the NLR Family Pyrin Domain Containing 3 (NLRP3) inflammasome within the lung.

Employing mRNA sequencing methods alongside *in vitro* analysis of alveolar macrophages (AMs) and T cells, our study elucidates a compelling correlation between $Terc^{ko/ko}$, inflammation, and impaired T cell functionality. Terc deletion results in compromised T cell function, characterized by dysregulation of the T cell receptor and absence of CD247, potentially compromising the host's capacity to mount an effective immune response against *S. aureus*.

This investigation provides insights into the intricate mechanisms governing increased vulnerability to severe pneumonia in the context of Terc deficiency, which might also contribute to aging-related pathologies, while also revealing for the first time the influence of Terc on T cell function.

Introduction

As the global population ages, the impact of infectious diseases on the aging population becomes increasingly significant. Among the most relevant risk factors leading to higher susceptibility as well as severity in both community-acquired (CA) and healthcare-associated (HA)-pneumonia is advanced age (≥ 60 years) (Torres et al., 2021). Particularly severe is pneumonia caused by *Staphylococcus aureus* (*S. aureus)* (Lee et al., 2022). *S. aureus* is a gram-positive bacterium that frequently colonizes humans but can manifest various pathologies, ranging from mild to more severe infections, including pneumonia (Howden et al., 2023; Jong, Kessel, & Strijp, 2019). It accounts for a notable proportion of CA and HA cases (Lee et al., 2022; Torres et al., 2021). The bacterium exhibits a broad spectrum of virulence factors, including toxins, adhesins, and immune evasion strategies, contributing to its ability to establish infections in the lower respiratory tract (Howden et al., 2023). Aging is a central factor predisposing individuals to a higher risk for *S. aureus* pneumonia (Torres et al., 2021). As aging is impacting several important functions of the body such as the immune response and thus the capability to mount an effective defensive response (Montecino-Rodriguez, Berent-Maoz, & Dorshkind, 2013). However, the aged immune system is also discussed to be more irritable, leading to a stronger inflammation after infection (Canan et al., 2014). This highlights the vital connection between aging and *S. aureus* pneumonia, as well as the need for further research investigating this connection.

The process of aging is a multifaceted phenomenon that involves various underlying mechanisms, known as hallmarks (López-Otín, Blasco, Partridge, Serrano, & Kroemer, 2023). Among these hallmarks, telomere shortening is a significant factor in cellular aging. Telomeres serve as protective caps at the end of

chromosomes, which shorten with every cell division until they reach a critical length where replication becomes impossible, eventually resulting in either apoptosis or senescence (López-Otín et al., 2023). However, this process can be counteracted by the telomerase, which can add new repeats to the ends of chromosomes and thus prevent the shortening of telomeres (Greider & Blackburn, 1985). The telomerase mainly consists of two parts: the telomerase reverse transcriptase (Tert), which harbors the enzymatic activity, and Terc, which serves as a template for the addition of new repeats (Sahin & DePinho, 2010; Shay & Wright, 2019).

One important aspect of telomere dysfunction is the impact of telomere shortening on the immune system as well as the hematopoietic system. Tissues or organ systems which are highly replicative are affected first by telomere shortening (Chakravarti, LaBella, & DePinho, 2021). Due to the loss of the protective telomere caps, mutations can accumulate, and the cells ultimately become senescent (Chakravarti et al., 2021). Interestingly, while most differentiated cells do not exhibit telomerase activity, T cells display a high activity of this enzyme (Hodes, Hathcock, & Weng, 2002). Aging T cells become senescent, which is characterized by short telomeres and the absence of CD28 expression (Hohensinner, Goronzy, & Weyand, 2011). Furthermore, telomere length and T cell functionality are closely connected. T cells with shorter telomeres are implicated in diseases related to aging like arthritis (Hohensinner et al., 2011). Additionally, $CD4^+$ T cells from Terc knockout ($Terc^{ko/ko}$) mice displayed several characteristics of aged T cells such as a reduction in CD28 expression and changed secretion of cytokines. Furthermore the naïve T cell population was reduced (Matthe, Thoma, Sperka, Neurath, & Waldner, 2022).This highlights the importance of intact telomeres and telomerase on immune cell function.

While most differentiated cells lack the expression of *Tert*, almost all human cells and several murine tissues express *Terc* (Zhang et al., 2018). However, the function of ubiquitous *Terc* expression remains elusive (Chakravarti et al., 2021; Shay & Wright, 2019). Interestingly, recent studies identified a variety of functions of Terc, which are independent of its function as part of the telomerase. Notably, a study could show that Terc triggers inflammation via the nuclear factor kappa-light-chain-enhancer of activated B cells (NF-κB) pathway (Liu, Yang, Ge, Liu, & Zhao, 2019). Furthermore, Terc was identified to be involved in cell proliferation by enhancing the expression of several genes belonging to the Phosphoinositide 3-kinase (Pi3K) – Protein Kinase B (AKT) pathway (Wu et al., 2022). The same study could show that this mechanism also contributed to $CD4^+$ T cell expansion (Wu et al., 2022). Additionally, *Terc* deletion in mice induced NLR Family Pyrin Domain Containing 3 NLRP3 inflammasome activation in macrophages upon pulmonary infection with *S. aureus*, thereby revealing another connection between immune modulation and the presence of Terc (Kang et al., 2018). Thus, it appears that Terc could serve as a relevant immunomodulatory factor, potentially implicated in *S. aureus*-induced pathologies.

Knockout of *Terc* in mice is a well-established model for premature aging, as telomeres of $Terc^{ko/ko}$ mice shorten with every generation (Wong et al., 2008). Additionally, the telomeres shorten during each generation with increasing age of the mice (Wong et al., 2008). Thus, while third-generation (G3) $Terc^{ko/ko}$ mice with already shortened telomeres were used in this study, they were infected at a young age (8 weeks). Enabling the possibility to study the effect of *Terc* deletion rather than telomere dysfunction. Furthermore, G3 $Terc^{ko/ko}$ mice with a C56Bl/6 background have a shorter lifespan, a smaller litter size and a generally reduced body size and weight (Wong et al., 2008).

120 In this study, we aimed to investigate the impact of *Terc* deletion, as an
121 essential immunomodulatory factor, on the immune response to *S. aureus*-induced
122 pneumonia in mice. For this purpose, G3 Terc$^{ko/ko}$ mice were infected with *S. aureus*,
123 and the progression of disease and immune response were evaluated. Strikingly, our
124 data highlights that the deletion of *Terc* resulted in a more severe disease outcome
125 and disrupted the innate and adaptive immune response. These findings suggest a
126 possible connection between Terc and immune cell homeostasis.

127 **Materials and Methods**

128 ***Bacteria***

129 All *in vivo* and *in vitro* experiments were carried out with the *S. aureus* strain
130 USA300. *S. aureus* was cultivated in brain heart infusion (BHI) medium (Thermo
131 Fisher Scientific, Waltham, MA, US) at 37°C while shaking at 150 rpm. The bacteria
132 were harvested during the mid-logarithmic phase and adjusted to the appropriate
133 optical density (OD) at 600nm for the respective experiments in phosphate-buffered
134 saline (PBS). The bacteria were then either used freshly for *in vivo* infection of mice
135 or stored at -80 °C until further usage in *in vitro* experiments.

136 For heat-killing, the adjusted bacteria stock was incubated at 95°C for 5 minutes
137 while shaking at 500 rpm. A fraction of the heat-killed bacteria was plated on Müller-
138 Hinton (MH) plates. Plates were incubated for 5 days at 37°C to confirm heat-killing
139 of the bacteria.

140 ***Determination of bacterial load***

141 Organs were homogenized in the appropriate amount of PBS (adjusted to their
142 weight in mg) using a SpeedMill Plus (Analytik Jena, Jena, Germany). Homogenized
143 organs and BAL fluid were diluted in a decadic dilution series and plated onto MH

144 plates. Plates were incubated overnight at 37°C. Colonies were counted, and colony-
145 forming units (CFU) per ml was calculated.

146 ***Mouse models and infection***

147 Mouse *in vivo* experiments were approved by the Office for Consumer Protection of
148 Thuringia (TV-Number: UKJ-19-028 and UKJ-22-023).

149 Third-generation (G3) female Terc$^{ko/ko}$ mice with a C57Bl/6 background were bred
150 from homozygous parents in the animal facility of the Jena University Hospital. To
151 confirm knockout of *Terc*, DNA was extracted from the tail of newborn mice using the
152 DNeasy Blood & Tissue Kit (Qiagen, Venlo, Netherlands) according to the
153 manufacturers protocol. The DNA was then used for genotyping via PCR using the
154 following primer sequences: mTR-R: 5´-TTC TGA CCA CCA CCA ACT TCA AT-3´;
155 mTR-WT-F: 5´-CTA AGC CGG CAC TCC TTA CAA G-3´; 5PPgK(-F): 5´-GGG GCT
156 GCT AAA GCG CAT-3´. The results were analyzed with an Agilent 2200 TapeStation
157 system using a Agilent D1000 ScreenTape (both Agilent Technologies, Santa Clara,
158 CA, USA). The WT *Terc* product had a size of 200 bp while the knockout product had
159 a size of 180 bp. Only mice that showed a single band at 180 bp were used for the
160 further breeding process. The Terc$^{ko/ko}$ mice were used for infection at the age of 8
161 weeks. Young WT (age 8 weeks) and old WT (age 24 months) C57Bl/6 mice were
162 purchased from Janvier Labs (Le Genest-Saint-Isle, France).

163 All mice were anesthetized with 2% isoflurane before intranasal infection with *S.*
164 *aureus* USA300 ($1x10^8$ CFU/ml) per mouse. After 24 hours, the mice were weighed
165 and scored as previously described (Hornung et al., 2023). Infected Terc$^{ko/ko}$ mice
166 were grouped into different degrees of severity based on their clinical score, fatal
167 outcome of the disease (fatal) and the presence of bacteria in organs other than the
168 lung (systemic infection). The mice were sacrificed via injection of an overdose of

169 xylazine/ketamine and bleeding of axillary artery. BAL was collected by instillation
170 and subsequent retrieval of PBS into the lungs. Blood and organs were collected.
171 The organs were stored at -80°C until further usage. Mice cohorts were not blinded to
172 those performing the experiments.

173

174 ***Telomere length measurement***

175 The length of telomeres in the lung of young WT, old WT and Terc$^{ko/ko}$ mice was
176 measured using the Absolute Mouse Telomere Length Quantification qPCR Assay Kit
177 (ScienCell research Laboratories, Carlsbad, CA, USA) according to the
178 manufacturer's protocol. Genomic DNA from the lungs was extracted by DNeasy
179 Blood & Tissue Kit (Qiagen, Venlo, Netherlands) according to the manufacturer's
180 protocol. For the PCR 2ng of each sample used. Average telomere length per
181 chromosome end was calculated as described by the manufacturer.

182

183 ***Histology and Immunofluorescence***

184 The left lung lobe was embedded into Tissue Tek O.C.T. (science services, Munich,
185 Germany) and stored at -80°C until further processing. Preparation and staining of
186 tissue cryosections was performed as described previously (Hornung et al., 2023).

187 For staining of *S. aureus,* rabbit anti- *S. aureus* polyclonal antibody (Cat. # PA1-7246,
188 Thermo Fisher Scientific, Waltham, MA, US) was diluted 1:400 in antibody diluent
189 with background reducing components (Agilent, Santa Clara, CA, US). Alexa Fluor®
190 488 AffiniPure Donkey Anti-Rabbit IgG (Cat. #711-545-152, Jackson Immuno
191 Research, West Grove, PA, US) and BODIPY 558/568 phalloidin, which stains actin
192 fibers, (Cat. # B3475, Thermo Fisher Scientific, Waltham, MA, US) were diluted in

193 antibody diluent 1:500 and 1:400 respectively and applied to the slides as secondary
194 antibodies.

195 ***Immunocytochemistry***

196 Murine primary macrophages were fixed with 4% paraformaldehyde (PFA) for 15
197 minutes at 37°C, subsequently permeabilized with 0.1% Triton-X, and blocked with
198 3% bovine serum albumin (BSA) in PBS for each 30 minutes at room temperature
199 (RT). Cells were incubated overnight with either rabbit anti- *S. aureus* polyclonal
200 antibody or rabbit anti-CD68 polyclonal antibody (Cat. # BOSSBS-0649R, VWR,
201 Radnor, PA, US) diluted 1:400 or 1:200 in 3% BSA in PBS respectively. The following
202 day, the slides were washed three times with PBS. Cy3-conjugated AffiniPure
203 Donkey Anti-Rabbit IgG (Cat. #711-165-152, Jackson Immuno Research, West
204 Grove, PA, US) and Alexa Fluor™Plus 647 Phalloidin (Cat. # A30107, Thermo Fisher
205 Scientific, Waltham, MA, US) were applied to the cells diluted 1:500 and 1:400 in 3%
206 BSA in PBS respectively and incubated for 1 hour at RT. The cells were then
207 mounted with DAPI Fluoromount-G.

208 The immunofluorescence pictures were taken with an AxioObserver Z.1 microscope
209 (Carl Zeiss AG, Oberkochen, Germany) and analyzed with the Zen software (Zen Pro
210 v3.3).

211 ***RNA extraction and mRNA sequencing***

212 RNA was extracted from murine lung tissue using the Trizol/Chloroform method. First,
213 about 15 mg of lung tissue was homogenized in TriZol LS reagent (Thermo Fisher
214 Scientific, Waltham, MA, US) using the SpeedMill Plus. The tissue-free supernatant
215 of the homogenate was transferred into a new tube after centrifugation. 50 µl of
216 chloroform was added to 250 µl TriZol Reagent, incubated for 3 minutes at RT, and

217 centrifuged at 12000xg for 15 minutes at 4°C. The aqueous phase was mixed with
218 isopropanol in a 1:2 ratio and incubated at RT for 10 minutes before centrifugation at
219 12000xg for 10 minutes at 4°C. Afterward, the RNA pellet was washed twice with
220 75% ethanol. Finally, ethanol was removed, and the pellet was air-dried for 5-10
221 minutes. The dry pellet was then dissolved in sterile distilled water, and RNA
222 concentration was determined by an ND-1000 NanoDrop spectrophotometer
223 (PEQLAB Biotechnologie GmbH, Erlangen, Germany). Before sequencing, RNA
224 integrity was measured using a 5400 Fragment Analyzer (Agilent Technologies,
225 Santa Clara, CA, US)) RNA concentration and RNA integrity of the samples can be
226 found in Supplemental Table 1.

227 Library construction and mRNA sequencing were performed by Novogene Co., LTD.
228 (Beijing, China) using the Illumina platform Novaseq 6000 S4 flowcell V1.0, based on
229 the sequencing by synthesis (SBS) mechanism and PE150 strategy. For
230 bioinformatics analysis, raw reads in FASTQ format were first processed using fastp.
231 Reads containing adapters and poly N sequences were removed as well as low
232 quality reads to generate clean data. Clean reads were then mapped to the reference
233 genome (Mus Musculus (GRCm39/mm39)) with the HISAT2 software. Gene
234 expression levels were quantified using the FPKM method. DESeq2 software as well
235 as negative binomial distribution was used for analysis of differential gene
236 expression. For FDR (False discovery rate) calculation the Benjamini-Hochberg
237 procedure was used. A summary of the quality of the sequencing data of each
238 sample can be found in Supplemental Table 2.

239 Heatmaps of the differentially regulated genes (DEG) were constructed using R
240 (v4.2.2; R Foundation for Statistical Computing, https://www.r-project.org/). Only
241 significant DEGs (p-value < 0.05) were displayed in the heatmaps. Non-significant

242 genes were set to zero and are shown in white. All DEGs used for construction of the
243 respective heatmaps are summarized in Supplemental Table 3a-i.

244 ***Immunophenotyping of the spleen***

245 Mice were sacrificed as described above, and spleens were freshly stored in cold 2%
246 FCS in PBS. For isolation of immune cells, spleens were mashed through a 70 µm
247 cell strainer (Miltenyi Biotec, Bergisch Gladbach, Germany), and red blood cell lysis
248 was performed by adding 5 ml of Ammonium–chloride–potassium (ACK) lysis buffer
249 (Thermo Fisher Scientific, Waltham, MA, US) for 5 minutes at 4°C to the pelleted
250 cells. Cells were then counted, adjusted to $2x10^6$ per ml PBS, and stained with BD
251 Fixable Viability Stain 780 (BD Biosciences, Heidelberg, Germany) diluted 1:1000 in
252 PBS for 15 minutes at RT. Unspecific binding of antibodies was blocked by incubating
253 the samples with 3% rat serum in BD staining buffer (BD Biosciences, Heidelberg,
254 Germany) for 5 minutes at RT. Anti-CD11c (Cat. #557401), anti-CD19 (Cat.
255 #566412), anti-CD335 (Cat. #564069), anti-CD34 (Cat. #742971), anti-CD3ε (Cat.
256 #553066), anti-Ly6G (Cat. #560601), and anti-F4/80 (Cat. #565411) were added to
257 the samples in a dilution of 1:100 and incubated for 20 minutes at 4°C. All antibodies
258 were purchased from BD Biosciences. Stained samples were measured with a BD
259 Symphony A1 (BD Biosciences, Heidelberg, Germany), and analysis was performed
260 with FlowJo v10.8.1. Detailed information on the gating strategy is presented in
261 Supplemental Figure 3A.

262 ***Isolation and infection of murine T cells and alveolar macrophages***

263 $Terc^{ko/ko}$ and young WT mice were sacrificed. Killing for scientific purposes was
264 conducted in accordance with the german animal welfare regulations. Alveolar
265 macrophages (AMs) were isolated as published elsewhere (Rios, Touyz, &
266 Montezano, 2017). In short, the murine lungs were washed out several times with

267 PBS containing 0.5 mM Ethylenediaminetetraacetic acid (EDTA). The lavage was
268 centrifuged at 350xg for 10 minutes at 4°C. The cell pellet was dissolved in Roswell
269 Park Memorial Institute (RPMI) medium containing 20 mM HEPES and 5% fetal calf
270 serum (FCS) and counted. Subsequently, cells were seeded and incubated at 37°C
271 for 2 hours.

272 Lymphocytes were isolated from the spleen as described above. To subsequently
273 isolate $CD4^+$ T cells, cells were separated via magnetic cell separation. These cells
274 were mixed with $CD4^+$ beads and separated via MACS LS Columns (both Miltenyi
275 Biotec, Bergisch Gladbach, Germany) according to the manufacturer's protocol. The
276 purity of the resulting $CD4^+$ T cell population was measured via flow cytometry using
277 a BD Symphony A1 (BD Biosciences, Heidelberg, Germany). T cells were added to
278 AMs for co-culture in a 1:1 ratio or cultured alone.

279 For infection with heat-killed (HK) *S. aureus,* a multiplicity of infection (MOI) of 5 was
280 calculated, and the appropriate bacteria volume was added to each well. Cells were
281 then incubated for 24 hours and harvested for downstream analysis.

282 ***Cytokine measurement***

283 For cytokine measurements, the lung tissue was homogenized using a SpeedMill
284 Plus in the appropriate volume of PBS to adjust the organs to their weight in mg.
285 Then, the cytokines were measured with the LEGENDPlex™ mouse inflammation
286 panel (BioLegend, San Diego, CA, US) according to the manufacturer's instructions.
287 Samples were run in duplicates on the same plate. For the young WT and $Terc^{ko/ko}$
288 cohort three biological replicates and for old WT cohorts four biological replicates
289 were measured. Supernatants of co-cultured and single-cultured T cells were
290 measured with the LEGENDPlex™ mouse T helper cytokine panel (BioLegend, San
291 Diego, CA, US). For each condition three biological replicates were measured. All

292 samples were run on the same plate. Flow cytometry analysis was performed with a
293 BD Symphony A1, and data analysis was carried out with the Qognit software v2023-
294 02-15 (BD Biosciences, Heidelberg, Germany).

295 ***Flow cytometry***

296 Co-cultured and single-cultured T cells were transferred to FACS tubes and
297 centrifuged at 500xg for 5 minutes at 4°C. The supernatant was frozen for cytokine
298 measurements, and the cell pellet was stained with PBS containing 1:1000 diluted
299 BD Fixable Viability Stain 780 (Cat. # 565388, BD Biosciences, Heidelberg,
300 Germany) for 15 minutes at RT. Staining of surface markers was performed as
301 described above. Samples were stained with anti- CD3ε (1:100, Cat. #553066), anti-
302 CD25 (1:800, Cat. #553866), anti-CD69 (1:400, Cat. # 551113) and anti-CD44
303 (1:100, Cat. # 560569) for 30 minutes at 4°C. All antibodies were purchased from BD
304 Pharmingen. Subsequently, samples were permeabilized and fixed. For this, the
305 samples were centrifuged for 5 minutes at 500xg and 4°C, resuspended in BD
306 Cytofix/Cytoperm buffer (BD Biosciences, Heidelberg, Germany), and incubated for
307 20 minutes at 4°C. Samples were washed once with BD Perm/Wash Buffer (BD
308 Biosciences, Heidelberg, Germany). For intracellular staining, samples were stained
309 with anti-CD247 (1:100, Cat. # ab91493, Abcam, Cambridge, UK) antibody in BD
310 Perm/Wash Buffer for 30 minutes at 4°C. Lastly, the samples were washed and
311 resuspended in BD Perm/Wash Buffer. Stained samples were measured with a BD
312 Symphony A1 and analyzed with FlowJo v10.8.1. Detailed information on the gating
313 strategy is presented in Supplemental Figure 3C.

314 ***Scanning electron microscopy (SEM)***

315 T cells and AMs were isolated as described above. Cells were grown on poly-L-lysine
316 (Merck-Millipore, Burlington, MA, US) coated glass coverslips in a 1:1 ratio. T cells

317 were allowed to attach to the coverslips for 30 minutes before adding *S. aureus*. After
318 adhesion of T cells, *S. aureus* USA300 was added at a MOI1 and incubated at 37°C.
319 After 3.5 hours, the samples were fixed with freshly prepared modified Karnovsky
320 fixative (4% w/v paraformaldehyde, 2.5 % v/v glutaraldehyde in 0.1 M sodium
321 cacodylate buffer, pH 7.4) for 1 hour at RT. After washing each 3 times for 15 minutes
322 with 0.1 M sodium cacodylate buffer (pH 7.4), the cells were post-fixed with 2% (w/v)
323 osmium tetroxide for 1 hour at RT. Subsequently, the samples were dehydrated in
324 ascending ethanol concentrations (30, 50, 70, 90, and 100%) for 15 minutes each.
325 Next, the samples were critical-point dried using liquid CO_2 and sputter coated with
326 gold (thickness approx. 2 nm) using a CCU-010 sputter coater (safematic GmbH,
327 Zizers, Switzerland). Finally, the specimens were investigated with a field emission
328 SEM LEO-1530 Gemini (Carl Zeiss NTS GmbH, Oberkochen, Germany).

329 ***Statistical analysis and scheme design***

330 Statistical analysis was carried out using GraphPad Prism 9. Illustrations were
331 created with BioRender.com.

332

333

334

335

336 **Results**

337 ***Terc* knockout is associated with severe pneumonia in mice**

338 To investigate the impact of Terc on the course of *S. aureus* pneumonia, we
339 used two murine aging models and compared them to young wild type (WT) mice.
340 For this purpose, we performed an intranasal infection of Terc$^{ko/ko}$ mice at the age of
341 8 weeks and naturally aged mice at the age of 2 years (old WT) with the *S. aureus*
342 strain USA300. WT mice at the age of 8 weeks (young WT) were additionally infected
343 and utilized as the control group (Figure 1A).

344 The clinical score of infected Terc$^{ko/ko}$ mice was increased compared to the
345 other two infected mice cohorts at 24 hours post infection (hpi) (Figure 1A). The
346 bacterial load was significantly higher in the bronchoalveolar lavage (BAL) of Terc$^{ko/ko}$
347 mice compared to old WT mice (Figure 1B). Interestingly, three distinct degrees of
348 severity were observed in the infected Terc$^{ko/ko}$ mice (n = 5): mild infection, systemic
349 infections, or fatal infections (Supplemental Figure 1A). Mice exhibiting systemic
350 infection were characterized by the presence of bacteria in extra pulmonary organs,
351 specifically observed in the liver and kidney tissues of some Terc$^{ko/ko}$ mice
352 (Supplemental Figure 1B).

353 Infection of young WT mice resulted in a significant decrease in bodyweight at
354 24 hpi. The body weight of infected Terc$^{ko/ko}$ mice was reduced compared to the
355 infected old WT mice and the non-infected Terc$^{ko/ko}$ mice (Figure 1C). In contrast, at
356 24 hpi the relative weight of the lung was increased in infected compared to the non-
357 infected mice for all cohorts, indicating inflammation of the lung (Figure 1D).
358 However, this effect was the most pronounced in young WT mice.

359 Based on our observation of the different degrees of severity displayed by the
360 infected Terc$^{ko/ko}$ mice, we categorized them according to their clinical score and the
361 presence of bacteria in extra pulmonary organs, distinguishing between mice with
362 and without systemic infection. This grouping resulted in more pronounced
363 differences between the mice cohorts regarding bacterial load and reduction of
364 relative body weight (Supplemental Figure 1C-D). The relative lung weight increased
365 for all groups compared to the respective non-infected mice, except for the Terc$^{ko/ko}$
366 mouse without systemic infection (Supplemental Figure 1E). Additionally, average
367 telomere length of the lungs of young and old WT as well as Terc$^{ko/ko}$ mice was
368 measured. As shortened telomeres are a hallmark of aging, impacting other cellular
369 mechanisms such as cellular senescence, they could have an influence on the
370 disease progression (López-Otín et al., 2023) . Notably, the telomeres of Terc$^{ko/ko}$
371 mice were the shortest among the three different mouse models, even shorter than
372 those of naturally aged mice (Supplemental Figure 1F).

373 In order to investigate gene expression patterns, mRNA sequencing of the
374 lungs was performed. This data supported the grouping of infected Terc$^{ko/ko}$ mice into
375 different groups, as the principal component analysis (PCA) plot showed a separate
376 cluster containing Terc$^{ko/ko}$ mice with systemic infection (Supplemental Figure 1G).

377 Immunofluorescence (IF) staining of *S. aureus* within the lung tissue of all
378 three infected mice cohorts was carried out. The increased signal for *S. aureus* in
379 sections of Terc$^{ko/ko}$ mice compared to sections of young WT and old WT mice closely
380 reflects the quantified CFU detected in the BAL (Figure 1E).

381 Terc$^{ko/ko}$ mice were characterized by an increased bacterial load in the lungs, a
382 higher clinical score as well as mortality (Figure 1A-B; Supplemental Figure 1A).
383 Additionally, we could observe different degrees of severity in the infected Terc$^{ko/ko}$

384 cohort and could identify a subgroup of mice with systemic infection (Supplemental
385 Figure 1A-B and G).

386 **Terc$^{ko/ko}$ mice showed excessive inflammation with inflammasome activation**

387 In order to investigate the underlying pathomechanisms leading to a more
388 severe course of disease in the Terc$^{ko/ko}$ mice, inflammation parameters in the lungs
389 were measured. In the course of this analysis, we applied the previously outlined
390 groups of mice, differentiating between those with and without systemic infection in
391 the Terc$^{ko/ko}$ cohort. Several pro-inflammatory cytokines were significantly
392 upregulated in Terc$^{ko/ko}$ mice with systemic infection, such as Interleukin-6 (IL-6),
393 Granulocyte-macrophage colony-stimulating factor (GM-CSF), and interleukin-1β (IL-
394 1β). Other important pro-inflammatory factors like Tumor necrosis factor α (TNFα)
395 and Interleukin-1α (IL-1α) were also elevated (Figure 2A). A significant upregulation
396 of pro-inflammatory mediators was, however, solely detected in infected Terc$^{ko/ko}$ mice
397 compared to the corresponding non-infected control cohort (Figure 2A).

398 We performed mRNA sequencing of the murine lung tissue to elucidate
399 potential differentially expressed genes that contribute to the more severe illness of
400 Terc$^{ko/ko}$ mice. Comparison of the gene expression profile of the different groups
401 revealed that non-infected young WT and Terc$^{ko/ko}$ mice cluster together and show a
402 similar expression profile. In contrast, the infected mice of those cohorts display
403 different expression patterns (Figure 2B). This highlights that most differences
404 between the knockout and WT mice are only present after infection with *S. aureus*.
405 Furthermore, both non-infected and infected old WT mice show a completely distinct
406 expression profile compared to young WT as well as Terc$^{ko/ko}$ mice (Figure 2B).

407 Intriguingly, several genes related to the NLRP3 inflammasome pathway, such
408 as *NLRP3* or Thioredoxin Interacting Protein *(TXNIP)*, were upregulated in infected

409 Terc$^{ko/ko}$, indicating activation of the inflammasome (Figure 2C; Supplemental Figure
410 2A). Notably, expression of genes encoding for TNFα, IL-1β, and IL-6 were
411 heightened. Thus, the increased inflammation in the lungs of Terc$^{ko/ko}$ mice is likely
412 induced by activation of the NLRP3 inflammasome (Figure 2C; Supplemental Figure
413 2A). Supporting this, the Nucleotide oligomerization domain (NOD)-like receptor
414 signaling pathway was among the most significantly enriched pathways when
415 comparing infected Terc$^{ko/ko}$ and young WT mice (Figure 2D).

416 Macrophages are part of the first line of defense against bacterial infections as
417 they can phagocytose bacteria and support pathogen clearance. AMs are present in
418 the lung and can directly react to the pathogen at the site of infection via the
419 production of inflammatory mediators or attraction of other immune cells (Malainou,
420 Abdin, Lachmann, Matt, & Herold, 2023). To specifically investigate the role of AMs
421 during *S. aureus* infection, we isolated them from lungs of young WT and Terc$^{ko/ko}$
422 mice. By using scanning electron microscopy (SEM) we could strikingly visualize the
423 ability of AMs to phagocytose *S. aureus* (Figure 3A). Additionally, we identified the
424 AMs via IF staining of the macrophage marker CD68 (Supplemental Figure 2B).

425 Notably, our sequencing data revealed an upregulation of pro-inflammatory M1
426 macrophage markers, such as C-X-C Motif Chemokine Ligand 2*(CXCL2)*, in Terc$^{ko/ko}$
427 mice following infection (Figure 3B; Supplemental Figure 2C). Anti-inflammatory M2
428 markers, e.g., Interferon Regulatory Factor 4 *(IRF4)*, were mainly downregulated.
429 Additionally, cluster of differentiation 14 *(CD14)*, a general macrophage marker, was
430 increased in the infected Terc$^{ko/ko}$ mice (Figure 3B; Supplemental Figure 2C).
431 Furthermore, the expression of multiple chemokines such as C-X-C Motif Ligand 1-3
432 *(CXCL1-3)* and C-C Motif Chemokine Ligand 2 *(CCL2)* was elevated, suggesting
433 increased migration of leukocytes such as macrophages and neutrophils to the lung

(Figure 3C; Supplemental Figure 2D). Additionally, the TNF, NF-κB and IL-17 signaling pathways were among the most significantly enriched pathways in infected Terc$^{ko/ko}$ mice compared to young WT mice (Figure 2D).

Combining the findings above, *S. aureus* infection in Terc$^{ko/ko}$ mice leads to excessive inflammation induced by NLRP3 inflammasome activation and infiltration of pro-inflammatory immune cells, such as M1 macrophages.

The T cell receptor is partially downregulated in infected Terc$^{ko/ko}$ mice

In addition to macrophages, T cells and their activation play a crucial role in the immune response and are vital for resolving infections. Surprisingly, multiple general T cell markers such as *CD2*, *CD5*, and *CD4* were downregulated in the infected Terc$^{ko/ko}$ mice compared to young WT mice (Figure 4A; Supplemental Figure 2E). However, these distinctions are not evident in comparisons between non-infected Terc$^{ko/ko}$ and young WT mice. This further emphasizes that the observed variations in immune response activation arise specifically in response to infection (Figure 4A). Some T cell markers, such as *CD5*, that were downregulated in infected Terc$^{ko/ko}$ mice were also downregulated in infected old WT mice compared to young WT mice (Supplemental Figure 2E).

To rule out that this effect is caused by a reduction of T cells in Terc$^{ko/ko}$ mice, the immune cells of non-infected Terc$^{ko/ko}$, young WT and old WT mice were analyzed via flow cytometry. However, no significant difference was observed between the groups (Figure 4B).

Additionally, several genes belonging to the T cell receptor (TCR) signaling pathway were downregulated in infected Terc$^{ko/ko}$ mice, such as *CD3G* (encoding CD3γ) and *CD247* encoding CD3ζ (Figure 4C, Supplemental Figure 2F).. Expression

458 of downstream factors of the TCR like Lymphocyte Cell-Specific Protein-Tyrosine
459 Kinase (*LCK*), linker of activation (*LAT*) and IL-2 inducible T cell kinase (*ITK*) was
460 also reduced (Figure 4C, Supplemental Figure 2F). We also noted several of these
461 distinctions, including the downregulation of *LCK* and *ITK* when comparing infected
462 old WT and young WT mice (Figure 4C). Since there was no reduction of T cells in
463 Terc$^{ko/ko}$ mice, the change in TCR signaling and marker expression is likely induced
464 by the infection.

465 Specifically, *CD247* was the only gene downregulated compared to infected
466 young WT, old WT, and non-infected Terc$^{ko/ko}$ mice (Figure 4C). Additionally, *CD247*
467 was downregulated in infected old WT mice compared to infected young WT mice
468 (Figure 4C). CD247 is an essential factor for the assembly of the TCR and the
469 downstream signaling after stimulation with an antigen (Jin, Yuan, Mehta, Ezenwa, &
470 Morel, 2024; Pitcher et al., 2003). In young WT mice gene expression levels of
471 *CD247* were increased with infection, likely due to proliferation and infiltration of T
472 cells. (Figure 4D). Notably, in infected Terc$^{ko/ko}$ mice, the expression of *CD247* is
473 absent. Moreover, there is no difference in *CD247* expression between non-infected
474 and infected old WT mice (Figure 4D). Similar trends can be seen for other T cell
475 markers, such as Programmed Cell Death 1 (*PDCD1*) and *CD4* (Figure 4E and F).
476 Additionally, the TCR signaling pathway and Th1 and Th2 differentiation pathway are
477 among the most enriched pathways in infected young WT mice compared to non-
478 infected young WT mice. In contrast, those pathways are not upregulated when
479 comparing infected Terc$^{ko/ko}$ with non-infected Terc$^{ko/ko}$ mice (Supplemental Figure
480 3B).

481 These findings indicate a malfunction in the activation of T cells as
482 components of the TCR signaling pathway were partially downregulated. The

483 complete absence of *CD247*, an essential factor for downstream activation of the
484 TCR, indicates aberrant T cell function of Terc$^{ko/ko}$ mice during infection.

485 **T cells of Terc$^{ko/ko}$ mice do not adequately react to infectious challenge**

486 To investigate the functionality of T cells and their CD247 expression in
487 Terc$^{ko/ko}$ mice during infection, murine T cells and AMs were isolated. Overstimulation
488 of T cells could be a potential explanation for the dysregulated TCR signaling.
489 Therefore, to study the impact of AMs on T cells we infected the co-culture of both
490 isolated cells with a multiplicity of infection 5 (MOI5) of heat-killed (HK) *S. aureus* for
491 24 hours (Figure 5A). All components of the experimental setup were visualized
492 using SEM. In particular, the close association between AMs and T cells was notable
493 (Figure 5B). IF staining of AMs of Terc$^{ko/ko}$ and young WT mice revealed the
494 successful internalization of *S. aureus* as well as a change of phenotypic appearance
495 to a more activated shape (Figure 5C).

496 Utilizing flow cytometry, we observed a substantial elevation in the baseline
497 expression of CD247 in T cells from Terc$^{ko/ko}$ mice in comparison to T cells from
498 young WT mice at 24 hpi (Figure 5D). However, there was no increase in CD247
499 expression upon stimulation with *S. aureus* in the Terc$^{ko/ko}$ T cells (Figure 5D). In
500 contrast, observation of T cells of young WT mice revealed a tendency towards an
501 increase in CD247 expression in response to *S. aureus* stimulation (Figure 5D). This
502 indicated improper activation of TCR signaling after *S. aureus* stimulation in T cells of
503 Terc$^{ko/ko}$ mice.

504 We could also detect differences in cytokine production when comparing the
505 AMs and T cells from young WT and Terc$^{ko/ko}$ mice. At 24 hpi, IL-1α production was
506 significantly higher in T cells from young WT mice stimulated with *S. aureus* when
507 compared to the T cells from Terc$^{ko/ko}$ mice (Figure 5D, left). Notably, in the co-

508 culture, IL-1α production was significantly higher in Terc$^{ko/ko}$ cells 2 hpi (Figure 5D,
509 right). On the contrary, there was a significant induction of IL-1α in the young WT co-
510 culture but no increase in the Terc$^{ko/ko}$ co-culture with *S. aureus* stimulation after 24
511 hours (Figure 5D, right).

512 Our data indicate that T cells from Terc$^{ko/ko}$ mice do not effectively react to the
513 infectious stimulus and thus seem dysfunctional due to TCR downregulation.

514

515 **Discussion**

516 Shortening of telomeres is a key factor in the aging process and has a
517 significant impact on other hallmarks of aging, such as mitochondrial dysfunction and
518 cellular senescence (Birch, Barnes, & Passos, 2018; López-Otín et al., 2023). In this
519 context, the discussion surrounding the importance of Terc is primarily confined to its
520 role within telomerase. Consequently, other potential functions of Terc in various
521 cellular processes have been largely overlooked. Interestingly, various studies have
522 linked Terc to inflammation, as it has been shown to activate the NF-κB and PI3K-
523 AKT pathways (Liu et al., 2019; Wu et al., 2022). Another study could show that the
524 deletion of *T*erc in mice resulted in NLRP3 inflammasome activation after infection
525 with *S. aureus*, thus contributing to more severe pneumonia (Kang et al., 2018).
526 These studies suggest a close association between Terc, inflammation, and the
527 response to bacterial lung infections.

528 In our study, we utilized a Terc$^{ko/ko}$ *S. aureus* pneumonia model to investigate
529 this connection. In accordance with german animal welfare regulations and the 3R
530 principle, we only had a reduced number of Terc$^{ko/ko}$ mice available for the
531 experiment, as some infections were fatal. This reduced number of mice is a
532 limitation of our study. However, we could demonstrate that Terc$^{ko/ko}$ mice presented
533 with a more severe pneumonia, higher bacterial load, and increased mortality
534 compared to old and young WT mice (Figure 1). Additionally, we could show that
535 infected Terc$^{ko/ko}$ mice are rather heterogeneous and display several degrees of
536 severity, which we investigated separately. Of 5 infected mice, 2 died, 2 displayed
537 signs of a systemic infection and only 1 had a mild infection. The mice with systemic
538 infection were grouped based on the presence of bacteria in organs other than the
539 lung, as well as the sequencing data, where they clustered separately. The in this

540 study conducted subclassification into different degrees of severity of Terc^{koko} mice is
541 lacking in similar studies, highlighting the here gained detailed insights. Terc$^{ko/ko}$ mice
542 were previously shown to have higher susceptibility to *S. aureus* pneumonia,
543 although they exhibited a reduced bacterial load in their lungs.(Kang et al., 2018).
544 These differences may be attributed to the missing separation of infected Terc$^{ko/ko}$
545 mice into different degrees of severity. Additionally, this heterogeneity in disease
546 manifestation points towards the limitations of mouse models to study *S. aureus*
547 pathologies. There are a variety of differences between *S. aureus* infections in
548 humans and mice. For instance several relevant virulence factors (e.g. Pantone-
549 Valentine leukocidine) function less efficient in mice than in humans (Zheng et al.,
550 2023). Therefore, higher infection doses are needed to successfully establish an
551 infection that is comparable to humans (Zheng et al., 2023).

552 Inflammation and the activation of the NLRP3 inflammasome are necessary
553 components to fight bacterial infections of the lung. However, excessive inflammation
554 and over-activation of the NLRP3 inflammasome lead to lung injury and can impede
555 pathogen clearance, thus contributing to *S. aureus*-induced pathologies (McVey,
556 Steinberg, & Goldenberg, 2021; Wang et al., 2022). Upon examining the lungs of
557 infected Terc$^{ko/ko}$ mice with systemic infection, we identified a marked increase in
558 inflammation parameters (Figure 2). Furthermore, we discovered that genes
559 associated with the NLRP3 inflammasome pathway were elevated in the infected
560 Terc$^{ko/ko}$ mice but not in the corresponding non-infected control cohort. As published
561 previously, this implies that *Terc* knockout on its own does not result in heightened
562 inflammation and inflammasome activation but rather requires an external trigger
563 (Kang et al., 2018). Inflammasome activation in Terc$^{ko/ko}$ mice was connected to
564 mitochondria dysfunction and an elevated reactive oxygen species (ROS) production.
565 Additionally, regulation of the inflammasome seems to be dysfunctional as TNAIFP3,

566 an important negative regulator of the inflammasome was downregulated in the
567 Terc$^{ko/ko}$ mice in this study (Kang et al., 2018). However, we did not observe
568 downregulation of TNFAIP3, but rather an upregulation in infected Terc$^{ko/ko}$ mice
569 (Figure 2C). These differences may however be attributed to the different study
570 design. Kang et al. focused on telomere dysfunction studying macrophages of old
571 Terc$^{ko/ko}$, while our study investigated the entire lung of young Terc$^{ko/ko}$ mice. Of
572 particular note were the heightened levels of IL-1β, a factor known for its ability to
573 amplify the inflammatory response and facilitate the infiltration of pro-inflammatory
574 immune cells, thereby fostering pulmonary injury (Chen et al., 2018; Hu et al., 2020).
575 Additionally, pro-inflammatory macrophages infiltrating the lung are critical to
576 inflammation-mediated lung injury (Chen et al., 2018; Guan, Zhou, Zhou, & Lin,
577 2023). In our study, we could identify the upregulation of several pro-inflammatory
578 macrophage markers in infected Terc$^{ko/ko}$ mice, as well as several chemokine
579 markers further exacerbating the inflammation in the lung via attraction of immune
580 cells (Figure 3). Notably, we did not observe upregulation of inflammation parameters
581 or activation of the inflammasome in the infected old WT mice. Although *CD14*
582 showed a slight increase in non-infected old WT mice compared to non-infected
583 young WT mice, there was no upregulation of macrophage markers in the infected
584 cohorts of these groups. Innate immune cells of aged individuals especially
585 macrophages are associated with chronic low grade inflammation contributing to
586 injury during infection (Duong et al., 2021). However studies could also show that
587 macrophages of aged mice had a reduced response to stimulation of pathogen
588 recognition receptors such as Toll-like receptor 2 (TLR2). This results in an initially
589 diminished and delayed response of macrophages to infectious challenge, which
590 could be a possible explanation for the lack of inflammation at 24 hpi (Boe, Boule, &
591 Kovacs, 2017; Hinojosa, Boyd, & Orihuela, 2009).

592 An overactive inflammatory response not only causes tissue damage but also
593 leads to T cell dysfunction (Guan et al., 2023). A possible mechanism is the
594 downregulation of CD247, which is the CD3ζ chain of the TCR. CD247/CD3ζ is
595 necessary for the assembly of the receptor at the cell surface. Furthermore due to its
596 multiple immunoreceptor tyrosine-based activation (ITAM) motifs, it is a central factor
597 in the signal transduction (Bronstein-Sitton et al., 2003; Jin et al., 2024). The
598 downregulation or absence of CD247/CD3ζ is linked to reduced responsiveness in T
599 cells and is commonly present in autoimmune diseases like rheumatoid arthritis and
600 lupus (Dexiu, Xianying, Yingchun, & Jiafu, 2022). This mechanism also occurs in
601 various chronic infectious diseases, including HIV and Hepatitis C (Dexiu et al.,
602 2022). However, it can also be a general regulatory process in T cells during
603 infection, helping to maintain immune homeostasis and prevent excessive
604 inflammation (Baniyash, 2004; van der Donk et al., 2021).Thus, the connection
605 between CD247/CD3ζ downregulation during chronic inflammation and chronic
606 infectious diseases has been well documented (Dexiu et al., 2022). Interestingly, we
607 could show that expression of *CD247* is entirely absent in infected Terc$^{ko/ko}$ mice,
608 while in the non-infected Terc$^{ko/ko}$ mice expression of *CD247* could be detected after
609 24 hours of infection. Hence, our data indicates that infection combined with deletion
610 of *Terc* is associated with reduction of *CD247* expression. Our study provides the first
611 evidence of the total absence of *CD247* expression during acute bacterial infection
612 and inflammation (Figure 4).

613 Previous work has already reported that constant stimulus with bacterial
614 antigens reduces the expression of CD247/CD3ζ and impairs T cell function
615 (Bronstein-Sitton et al., 2003). However, the complete absence of CD247/CD3ζ after
616 a single antigenic stimulus, without chronic inflammation as well as the connection to

617 knockout of *Terc*, are novel findings. These findings require further studies and
618 investigations to gain a deeper understanding of the underlying mechanisms.

619 Downregulation of CD247/CD3ζ is facilitated by myeloid suppressor cells
620 (MSC), which accumulate at the site of inflammation (Baniyash, 2004; Dexiu et al.,
621 2022; Ezernitchi et al., 2006). MSC are cells which exert an immunosuppressive
622 function on T cells in response to inflammation or infection (Medina & Hartl, 2018).
623 Thus MSC contribute towards the regulation of the immune response to pathogens to
624 prevent an overshooting reaction of the immune system (Medina & Hartl, 2018).
625 However their immunosuppressive function can also exacerbate infections. For
626 instance, elevated levels of MSC induced T cell dysfunctionality and caused an
627 exacerbated and sustained chronic infection in an *S. aureus* mouse model (Tebartz et
628 al., 2015). Immunosuppression of T cells is conveyed by multiple mechanisms, one
629 of which is the downregulation of CD247/CD3ζ (Ezernitchi et al., 2006). This process
630 is facilitated among others by the ability of MSCs to metabolize the amino acid
631 arginine, as arginine seems to be essential for expression of CD247 in T cells
632 (Ezernitchi et al., 2006; Rodriguez et al., 2004). Interestingly, we could identify
633 several MSC markers, such as lymphocyte antigen 6 family member G (*LY6G)*, to be
634 upregulated in the infected $Terc^{ko/ko}$ mice. This suggests a potential role of MSCs in
635 the downregulation of CD247/CD3ζ (Supplemental Figure 3E). Notably, we could
636 identify reduced expression of *CD247* in infected old WT mice compared to young
637 WT mice. Moreover, our sequencing data did not show an increase in *CD247*
638 expression in infected old WT mice compared to the non-infected control group,
639 which further suggests that the T cells of old WT mice may also exhibit some level of
640 dysfunction (Figure 4). One potential underlying mechanism is the reduced ability of
641 aged macrophages to activate T cells due to diminished expression of the receptor
642 required for presentation of the antigen (Herrero, Marqués, Lloberas, & Celada,

643 2001). Furthermore, T cells of aged individuals become increasingly deficient due to
644 immunosenescence and exhaustion (Mittelbrunn & Kroemer, 2021). Supporting this,
645 we could observe downregulation of *CD27* compared to infected Young WT mice
646 respectively, while *CTLA4* was upregulated in infected old WT compared to
647 uninfected mice (Supplemental Figure 2E and F). Downregulation of CD28 and CD27
648 is part of T cell aging and an essential marker of T cell senescence, while
649 upregulation of CTLA4 is part of a signature pointing to T cell exhaustion (Zhao,
650 Shao, & Peng, 2020). Interestingly, senescent T cells have shorter telomeres and
651 exhibit reduced telomerase activity, which indicates a possible connection between
652 Terc and T cell function (Mittelbrunn & Kroemer, 2021). Interestingly, *CD28*
653 expression was downregulated in infected Terc$^{ko/ko}$ mice compared to old WT infected
654 mice (Figure 4A and C). However, we did not observe any other relevant changes of
655 T cell senescence or exhaustion markers in infected Terc$^{ko/ko}$ mice (Figure 4A and C).
656 Thus T cell senescence could be a contributing factor to the T cell dysfunctionality,
657 but likely does not explain the complete phenotype. The differences in the expression
658 of T cell senescence and exhaustion markers, in addition to the lack of increased
659 inflammation in old WT mice, indicates that mechanisms causing downregulation of
660 parts of the TCR and T helper cell markers in old WT and Terc$^{ko/ko}$ mice differ from
661 each other. As T cell senescence is however a known consequence of *Terc* deletion,
662 the lack of in depth investigation of this process in the present study is a limitation
663 (Matthe et al., 2022). Further experiments investigating the role of T cell senescence
664 in this model should therefore be conducted.

665 Hence, old WT mice exhibit certain immune cell dysfunction similarities.
666 However, given the intricate nature of aging, other mechanisms contribute to the
667 distinct response observed in Terc$^{ko/ko}$ and old WT mice following infection. This
668 highlights the necessity of employing a knockout model to specifically examine the

669 influence of Terc on infection, isolating it from the multifaceted processes involved in
670 aging.

671 We observed an increase in pro-inflammatory macrophages in the lungs of
672 Terc$^{ko/ko}$ mice during infection. To explore the role of macrophages in regulating T cell
673 function during infection, we investigated whether AMs were sufficient to induce
674 CD247/CD3ζ downregulation in T cells. While CD247/CD3ζ expression increased
675 with bacterial stimulation in T cells from young WT mice, we failed to induce such an
676 increase in CD247/CD3ζ expression in T cells from Terc$^{ko/ko}$ mice (Figure 5). The
677 expression pattern of CD247/CD3ζ was similar to that observed in the sequencing
678 data, as initial levels of CD247/CD3ζ expression in non-infected Terc$^{ko/ko}$ mice were
679 higher than those of young WT mice. However, there was no significant reduction of
680 CD247/CD3ζ after stimulation with bacteria in the T cells of Terc$^{ko/ko}$ mice. One
681 potential explanation for this finding is the absence of MSCs and other infiltrating
682 cells, which can contribute to the inflammatory environment and lead to T cell
683 dysfunction. Furthermore, after 24 but not 2 hours of infection, we observed a
684 reduced release of the pro-inflammatory cytokine IL-1α from Terc$^{ko/ko}$ T cells,
685 suggesting a time-dependent reduction of T cell function. The results of the
686 experiment conducted on T cells of Terc$^{ko/ko}$ mice revealed an insufficient response to
687 the bacterial stimulation, as there was no significant increase in CD247/CD3ζ
688 expression or IL-1α release after 24 hpi. However, additional experiments are needed
689 to validate and further investigate the underlying mechanisms leading to T cell
690 dysfunctionality in Terc$^{ko/ko}$ mice.

691 Our data points towards the pivotal role of Terc in the regulation of
692 inflammation as well as maintaining immune homeostasis during infection. We could
693 demonstrate that *S. aureus* pneumonia in Terc$^{ko/ko}$ mice resulted in an overshooting

694 inflammation and activation of the NLRP3 inflammasome. The elevated inflammation
695 eventually leads to T cell dysfunction, which impairs the host's ability to mount an
696 effective immune response against the pathogen, resulting in increased bacterial load
697 and mortality. As T cell dysfunctionality is caused by the excessive inflammation,
698 other pathogens inducing high inflammatory responses in the host could also lead to
699 a similar phenotype in Terc$^{ko/ko}$ mice.

700 This study linked T cell dysfunction to Terc deletion for the first time and thus
701 provided insights into possible mechanisms contributing to a more severe *S. aureus*
702 pneumonia in the aging population.

703 **Acknowledgments**

704 Breeding pairs of Terc$^{ko/ko}$ mice were kindly provided by Lenhard Rudolph (Leibniz
705 Institute on Aging, Jena, Germany). We thank Sylvia Hänßgen, Yvonne Ozegowski,
706 and Lea Herrmann for their excellent technical assistance.

707 **Conflicts of interest**

708 The authors declare that the research was conducted in the absence of any
709 commercial or financial relationships that could be construed as a potential conflict of
710 interest.

711 **Funding**

712 This work is supported by the BMBF, funding program Photonics Research Germany
713 ("LPI-BT1-FSU", FKZ 13N15466; "LPI-BT2-IPHT", FKZ 13N15704) and is integrated
714 into the Leibniz Center for Photonics in Infection Research (LPI). The LPI initiated by
715 Leibniz-IPHT, Leibniz-HKI, UKJ, and FSU Jena is part of the BMBF national roadmap
716 for research infrastructures. We also want to thank the BMBF for the funding for the
717 "ADA" (13GW0456A). In addition, this work was supported by funding from the

Foundation "Else Kröner-Fresenius-Stiftung" within the Else Kröner Graduate School for Medical Students "Jena School for Ageing Medicine (JSAM). This research was also supported by the Deutsche Forschungsgemeinschaft (DFG, German Research Foundation) under Germany's Excellence Strategy-EXC 2051 (Project ID No. 390713860).

Author Contributions

Conceptualization, S.D.-E.; methodology, Y.R; F.H., A.H., T.L., S.N., writing—original draft preparation, Y.R.; S.D.-E. writing—review and editing, all authors; visualization: Y.R., S.D.-E.; resources and supervision: B.L., S.D.-E.; funding acquisition, B.L.; S.D.-E. All authors have read and agreed to the published version of the manuscript.

Data availability statement

The data supporting this study's findings are available from the corresponding author upon reasonable request.

References

Baniyash, M. (2004). TCR ζ-chain downregulation: curtailing an excessive inflammatory immune response. *Nature Reviews Immunology, 4*(9), 675-687. doi:10.1038/nri1434

Birch, J., Barnes, P. J., & Passos, J. F. (2018). Mitochondria, telomeres and cell senescence: Implications for lung ageing and disease. *Pharmacology & Therapeutics, 183*, 34-49. doi:https://doi.org/10.1016/j.pharmthera.2017.10.005

Boe, D. M., Boule, L. A., & Kovacs, E. J. (2017). Innate immune responses in the ageing lung. *Clin Exp Immunol, 187*(1), 16-25. doi:10.1111/cei.12881

Bronstein-Sitton, N., Cohen-Daniel, L., Vaknin, I., Ezernitchi, A. V., Leshem, B., Halabi, A., . . . Baniyash, M. (2003). Sustained exposure to bacterial antigen induces interferon-γ-dependent T cell receptor ζ down-regulation and impaired T cell function. *Nature Immunology, 4*(10), 957-964. doi:10.1038/ni975

Canan, C. H., Gokhale, N. S., Carruthers, B., Lafuse, W. P., Schlesinger, L. S., Torrelles, J. B., & Turner, J. (2014). Characterization of lung inflammation and its impact on macrophage function in aging. *Journal of Leukocyte Biology, 96*(3), 473-480. doi:10.1189/jlb.4A0214-093RR

Chakravarti, D., LaBella, K. A., & DePinho, R. A. (2021). Telomeres: history, health, and hallmarks of aging. *Cell, 184*(2), 306-322. doi:https://doi.org/10.1016/j.cell.2020.12.028

Chen, J., Wang, S., Fu, R., Zhou, M., Zhang, T., Pan, W., . . . Huang, Y. (2018). RIP3 dependent NLRP3 inflammasome activation is implicated in acute lung injury in mice. *Journal of Translational Medicine, 16*(1), 233. doi:10.1186/s12967-018-1606-4

Dexiu, C., Xianying, L., Yingchun, H., & Jiafu, L. (2022). Advances in CD247. *Scand J Immunol, 96*(1), e13170. doi:10.1111/sji.13170

Duong, L., Radley, H. G., Lee, B., Dye, D. E., Pixley, F. J., Grounds, M. D., . . . Jackaman, C. (2021). Macrophage function in the elderly and impact on injury repair and cancer. *Immunity & Ageing, 18*(1), 4. doi:10.1186/s12979-021-00215-2

Ezernitchi, A. a. V., Vaknin, I., Cohen-Daniel, L., Levy, O., Manaster, E., Halabi, A., . . . Baniyash, M. (2006). TCR ζ Down-Regulation under Chronic Inflammation Is Mediated by Myeloid Suppressor Cells Differentially Distributed between Various Lymphatic Organs1. *The Journal of Immunology, 177*(7), 4763-4772. doi:10.4049/jimmunol.177.7.4763

Greider, C. W., & Blackburn, E. H. (1985). Identification of a specific telomere terminal transferase activity in Tetrahymena extracts. *Cell, 43*(2 Pt 1), 405-413. doi:10.1016/0092-8674(85)90170-9

Guan, T., Zhou, X., Zhou, W., & Lin, H. (2023). Regulatory T cell and macrophage crosstalk in acute lung injury: future perspectives. *Cell Death Discovery, 9*(1), 9. doi:10.1038/s41420-023-01310-7

Herrero, C., Marqués, L., Lloberas, J., & Celada, A. (2001). IFN-gamma-dependent transcription of MHC class II IA is impaired in macrophages from aged mice. *J Clin Invest, 107*(4), 485-493. doi:10.1172/jci11696

Hinojosa, E., Boyd, A. R., & Orihuela, C. J. (2009). Age-associated inflammation and toll-like receptor dysfunction prime the lungs for pneumococcal pneumonia. *J Infect Dis, 200*(4), 546-554. doi:10.1086/600870

Hodes, R. J., Hathcock, K. S., & Weng, N.-p. (2002). Telomeres in T and B cells. *Nature Reviews Immunology, 2*(9), 699-706. doi:10.1038/nri890

Hohensinner, P. J., Goronzy, J. J., & Weyand, C. M. (2011). Telomere dysfunction, autoimmunity and aging. *Aging Dis, 2*(6), 524-537. Retrieved from https://www.ncbi.nlm.nih.gov/pmc/articles/PMC3295061/pdf/ad-2-6-524.pdf

Hornung, F., Schulz, L., Köse-Vogel, N., Häder, A., Grießhammer, J., Wittschieber, D., . . . Deinhardt-Emmer, S. (2023). Thoracic adipose tissue contributes to severe virus infection of the lung. *International Journal of Obesity, 47*(11), 1088-1099. doi:10.1038/s41366-023-01362-w

Howden, B. P., Giulieri, S. G., Wong Fok Lung, T., Baines, S. L., Sharkey, L. K., Lee, J. Y. H., . . . Stinear, T. P. (2023). Staphylococcus aureus host interactions and adaptation. *Nature Reviews Microbiology, 21*(6), 380-395. doi:10.1038/s41579-023-00852-y

Hu, X., Qin, H., Li, Y., Li, J., Fu, L., Li, M., . . . Yin, B. (2020). Biochanin A protect against lipopolysaccharide-induced acute lung injury in mice by regulating TLR4/NF-κB and PPAR-γ pathway. *Microbial Pathogenesis, 138*, 103846. doi:https://doi.org/10.1016/j.micpath.2019.103846

Jin, Y., Yuan, H., Mehta, I., Ezenwa, O., & Morel, P. A. (2024). Alternatively Spliced Variants of Murine CD247 Influence T Cell Development and Activation, Revealing the Importance of the CD3ζ C-Terminal Region. *J Immunol, 212*(4), 541-550. doi:10.4049/jimmunol.2300511

Jong, N. W. M. d., Kessel, K. P. M. v., & Strijp, J. A. G. v. (2019). Immune Evasion by *Staphylococcus aureus*. *Microbiology Spectrum, 7*(2), 10.1128/microbiolspec.gpp1123-0061-2019. doi:doi:10.1128/microbiolspec.gpp3-0061-2019

Kang, Y., Zhang, H., Zhao, Y., Wang, Y., Wang, W., He, Y., . . . Shi, L. (2018). Telomere Dysfunction Disturbs Macrophage Mitochondrial Metabolism and the NLRP3 Inflammasome through the PGC-1α/TNFAIP3 Axis. *Cell Reports, 22*(13), 3493-3506. doi:https://doi.org/10.1016/j.celrep.2018.02.071

Lee, L.-N., Chou, W.-R., Wang, J.-Y., Kuo, Y.-L., Chang, C.-Y., Lee, Y.-C., . . . Liu, W.-L. (2022). Characteristics and local risk factors of community-acquired and health-care-associated Staphylococcus aureus pneumonia. *Scientific Reports, 12*(1), 18670. doi:10.1038/s41598-022-23246-1

Liu, H., Yang, Y., Ge, Y., Liu, J., & Zhao, Y. (2019). TERC promotes cellular inflammatory response independent of telomerase. *Nucleic Acids Research, 47*(15), 8084-8095. doi:10.1093/nar/gkz584

López-Otín, C., Blasco, M. A., Partridge, L., Serrano, M., & Kroemer, G. (2023). Hallmarks of aging: An expanding universe. *Cell, 186*(2), 243-278. doi:https://doi.org/10.1016/j.cell.2022.11.001

Malainou, C., Abdin, S. M., Lachmann, N., Matt, U., & Herold, S. (2023). Alveolar macrophages in tissue homeostasis, inflammation, and infection: evolving concepts of therapeutic targeting. *The Journal of Clinical Investigation, 133*(19). doi:10.1172/JCI170501

Matthe, D. M., Thoma, O. M., Sperka, T., Neurath, M. F., & Waldner, M. J. (2022). Telomerase deficiency reflects age-associated changes in CD4+ T cells. *Immun Ageing, 19*(1), 16. doi:10.1186/s12979-022-00273-0

McVey, M. J., Steinberg, B. E., & Goldenberg, N. M. (2021). Inflammasome activation in acute lung injury. *American Journal of Physiology-Lung Cellular and Molecular Physiology, 320*(2), L165-L178. doi:10.1152/ajplung.00303.2020

Medina, E., & Hartl, D. (2018). Myeloid-Derived Suppressor Cells in Infection: A General Overview. *J Innate Immun, 10*(5-6), 407-413. doi:10.1159/000489830

Mittelbrunn, M., & Kroemer, G. (2021). Hallmarks of T cell aging. *Nature Immunology, 22*(6), 687-698. doi:10.1038/s41590-021-00927-z

Montecino-Rodriguez, E., Berent-Maoz, B., & Dorshkind, K. (2013). Causes, consequences, and reversal of immune system aging. *The Journal of Clinical Investigation, 123*(3), 958-965. doi:10.1172/JCI64096

Pitcher, L. A., Young, J. A., Mathis, M. A., Wrage, P. C., Bartók, B., & Van Oers, N. S. C. (2003). The formation and functions of the 21- and 23-kDa tyrosine-phosphorylated TCR ζ subunits. *Immunological Reviews, 191*(1), 47-61. doi:https://doi.org/10.1034/j.1600-065X.2003.00003.x

Rios, F. J., Touyz, R. M., & Montezano, A. C. (2017). Isolation and Differentiation of Murine Macrophages. In R. M. Touyz & E. L. Schiffrin (Eds.), *Hypertension: Methods and Protocols* (pp. 297-309). New York, NY: Springer New York.

Rodriguez, P. C., Quiceno, D. G., Zabaleta, J., Ortiz, B., Zea, A. H., Piazuelo, M. B., . . . Ochoa, A. C. (2004). Arginase I Production in the Tumor Microenvironment by Mature Myeloid Cells Inhibits T-Cell Receptor Expression and Antigen-Specific T-Cell Responses. *Cancer Research, 64*(16), 5839-5849. doi:10.1158/0008-5472.Can-04-0465

Sahin, E., & DePinho, R. A. (2010). Linking functional decline of telomeres, mitochondria and stem cells during ageing. *Nature, 464*(7288), 520-528. doi:10.1038/nature08982

Shay, J. W., & Wright, W. E. (2019). Telomeres and telomerase: three decades of progress. *Nature Reviews Genetics, 20*(5), 299-309. doi:10.1038/s41576-019-0099-1

Tebartz, C., Horst, S. A., Sparwasser, T., Huehn, J., Beineke, A., Peters, G., & Medina, E. (2015). A major role for myeloid-derived suppressor cells and a minor role for regulatory T cells in immunosuppression during Staphylococcus aureus infection. *J Immunol, 194*(3), 1100-1111. doi:10.4049/jimmunol.1400196

Torres, A., Cilloniz, C., Niederman, M. S., Menéndez, R., Chalmers, J. D., Wunderink, R. G., & van der Poll, T. (2021). Pneumonia. *Nature Reviews Disease Primers, 7*(1), 25. doi:10.1038/s41572-021-00259-0

van der Donk, L. E. H., Ates, L. S., van der Spek, J., Tukker, L. M., Geijtenbeek, T. B. H., & van Heijst, J. W. J. (2021). Separate signaling events control TCR downregulation and T cell activation in primary human T cells. *Immun Inflamm Dis, 9*(1), 223-238. doi:10.1002/iid3.383

Wang, Y., Cao, C., Zhu, Y., Fan, H., Liu, Q., Liu, Y., . . . Wu, M. (2022). TREM2/β-catenin attenuates NLRP3 inflammasome-mediated macrophage pyroptosis to promote bacterial clearance of pyogenic bacteria. *Cell Death & Disease, 13*(9), 771. doi:10.1038/s41419-022-05193-x

Wong, L. S. M., Oeseburg, H., de Boer, R. A., van Gilst, W. H., van Veldhuisen, D. J., & van der Harst, P. (2008). Telomere biology in cardiovascular disease: the TERC−/− mouse as a model for heart failure and ageing. *Cardiovascular Research, 81*(2), 244-252. doi:10.1093/cvr/cvn337

Wu, S., Ge, Y., Lin, K., Liu, Q., Zhou, H., Hu, Q., . . . Ju, Z. (2022). Telomerase RNA TERC and the PI3K-AKT pathway form a positive feedback loop to regulate cell proliferation independent of telomerase activity. *Nucleic Acids Res, 50*(7), 3764-3776. doi:10.1093/nar/gkac179

Zhang, M. W., Zhao, P., Yung, W. H., Sheng, Y., Ke, Y., & Qian, Z. M. (2018). Tissue iron is negatively correlated with TERC or TERT mRNA expression: A heterochronic parabiosis study in mice. *Aging (Albany NY), 10*(12), 3834-3850. doi:10.18632/aging.101676

Zhao, Y., Shao, Q., & Peng, G. (2020). Exhaustion and senescence: two crucial dysfunctional states of T cells in the tumor microenvironment. *Cellular & Molecular Immunology, 17*(1), 27-35. doi:10.1038/s41423-019-0344-8

Zheng, P., Liu, F., Long, J., Jin, Y., Chen, S., Duan, G., & Yang, H. (2023). Latest Advances in the Application of Humanized Mouse Model for Staphylococcus aureus. *The Journal of Infectious Diseases, 228*(6), 800-809. doi:10.1093/infdis/jiad253

869 **Figure Legends**

870 **Figure 1: Terc$^{ko/ko}$ mice exhibit more severe pneumonia with increased mortality**
871 **and a higher bacterial load.**

872 A) Clinical score of non-infected and infected young WT (n =10, 5 non-infected and 5
873 infected), old WT (n =10, 5 non-infected and 5 infected), and Terc$^{ko/ko}$ (n =8, 3 non-
874 infected and 5 infected) mice. The age and genetic background of the different
875 groups is depicted below.

876 B) Bacterial load of the lungs of infected mice at 24 hpi. Data is displayed as
877 logarithmic.

878 C) Relative body weight of young WT, old WT and Terc$^{ko/ko}$ mice. Relative body
879 weight displays body weight at 24 hpi as a percentage of the body weight at the time
880 of infection.

881 D) Relative lung weight of young WT, old WT, and Terc$^{ko/ko}$ mice. Relative lung weight
882 displays lung weight at 24 hpi as a percentage of the current body weight.

883 E) Immunofluorescence staining of lung tissue of infected young (WT 8 weeks), old
884 (WT 2 years), and Terc$^{ko/ko}$ mice. Lungs were stained for *S. aureus* (green), actin
885 (red), and DAPI (blue). Representative pictures are shown for each group.

886 *$p < 0.05$, **$p < 0.01$, ***$p<0.001$. P calculated by Kruskal-Wallis-test (A-D). Each
887 replicate is displayed as a data point.

888 **Figure 2: Lungs of Terc$^{ko/ko}$ mice display excessive inflammation and NLRP3**
889 **inflammasome activation.**

890 A) Pro-inflammatory cytokines measured in the lungs of non-infected and infected
891 young WT (each n=3), old WT (each n=4) and Terc$^{ko/ko}$ mice (non-infected: n=3, with

892 systemic infection: n=2 and infected: n=1). Infected Terc$^{ko/ko}$ mice were grouped into
893 with systemic and without systemic infection. Data is displayed on a logarithmic
894 scale.

895 B) Heatmap of overall gene expression in the different mice cohorts analyzed. Gene
896 expression is displayed as the log2 of the fragments per kilobase of transcript per
897 million fragments mapped (fpkm) of each individual gene. Red indicates upregulation,
898 and green indicates downregulation of the gene expression. The respective mouse
899 groups are visualized above the heatmap. For each mouse cohort three biological
900 replicates were sequenced.

901 C) Heatmap of differentially expressed genes (DEG) belonging to the NLRP3
902 inflammasome pathway. Red indicates upregulation, and blue indicates
903 downregulation of the gene. Differential gene expression analysis was conducted
904 using the DESeq2 software as well as negative binomial distribution. For FDR
905 calculation the Benjamini-Hochberg procedure was used. Heatmaps were
906 constructed using R Studio. Only significant DEGs (p-value < 0.05) were displayed in
907 the heatmap. Non-significant genes were set to zero and are shown as white. DEGs
908 are displayed as log2fold-change. For each group three biological replicates were
909 sequenced and used for analysis. For clarity, the heatmap has been split in half, and
910 no column clustering has been performed. The respective groups used for the
911 comparison are indicated below each column.

912 D) Overview of the most differentially enriched KEGG pathways between infected
913 young and Terc$^{ko/ko}$ mice. The dot plot was constructed using R Studio.

914 ns ≥ 0.05, *p < 0.05, **p < 0.01, ***p<0.001, ****p < 0.0001. P calculated by Kruskal-
915 Wallis-test (A). Each replicate is displayed as a data point.

916 **Figure 3: Elevated expression of pro-inflammatory M1 macrophages markers**
917 **and chemokines are present in the lungs of infected Terc$^{ko/ko}$ mice.**

918 A) Colorized SEM picture of an AM from young WT mice during phagocytosis of *S.*
919 *aureus.*

920 Heatmap of differentially expressed macrophage markers (B) and DEGs belonging to
921 the chemokine signaling pathway (C). Red indicates upregulation, and blue indicates
922 downregulation of the gene. Differential gene expression analysis was conducted
923 using the DESeq2 software as well as negative binomial distribution. For FDR
924 calculation the Benjamini-Hochberg procedure was used. Heatmaps were
925 constructed using R Studio. Only significant DEGs (p-value < 0.05) were displayed in
926 the heatmap. Non-significant genes were set to zero and are shown as white. DEGs
927 are displayed as log2fold-change. For each group three biological replicates were
928 sequenced and used for analysis. The respective groups used for the comparison are
929 indicated below each column.

930 **Figure 4**: **TCR in infected Terc$^{ko/ko}$ mice is partially downregulated.**

931 Heatmap of differentially expressed T helper cell markers (A) and DEGs belonging to
932 the TCR signaling pathway (C). Red indicates upregulation, and blue indicates
933 downregulation of the gene. Differential gene expression analysis was conducted
934 using the DESeq2 software as well as negative binomial distribution. For FDR
935 calculation the Benjamini-Hochberg procedure was used. Heatmaps were
936 constructed using R Studio. Only significant DEGs (p-value < 0.05) were displayed in
937 the heatmap. Non-significant genes were set to zero and are shown as white. DEGs
938 are displayed as log2fold-change. For each mouse cohort three biological replicates
939 were sequenced and used for analysis. The respective groups used for the
940 comparison are indicated below each column.

941 B) Percentage of $CD3^+$ -living cells in non-infected young WT (n=3), old WT (n=3),
942 and $Terc^{ko/ko}$ mice (n=5) spleen. Cells were analyzed with flow cytometry.

943 Gene expression levels in fpkm of *CD247* (D), *PDCD1* (E), and *CD4* (F) in young WT
944 (n=3), old WT (n=3), and $Terc^{ko/ko}$ mice (n=3).

945 ns ≥ 0.05, *p < 0.05, **p < 0.01. P calculated by Kruskal-Wallis-test (B; D-F). Each
946 replicate is displayed as a data point.

947 **Figure 5**: **T cells of $Terc^{ko/ko}$ mice do not adequately react to bacterial challenge.**

948 (A) Schematic representation of experiment. Murine T cells and AMs were isolated,
949 co-cultured, and stimulated with heat-killed *S. aureus* with an MOI5 for 24 hours.

950 (B) Colorized SEM picture of the experimental setup. An AM close to a T cell, is
951 shown.

952 (C) Immunofluorescence staining of infected and non-infected AMs from young WT
953 and $Terc^{ko/ko}$ mice. AMs were stained with antibodies for *S. aureus* (red), actin
954 (purple), and DAPI (blue).

955 (D) CD247 expression measured with flow cytometry of non-infected and infected T
956 cells (left) and co-cultured T cells and AMs (right) of young WT (each n=3) and
957 $Terc^{ko/ko}$ mice (each n=3) after 24 hpi. CD247 expression is displayed as geometric
958 mean fluorescence intensity (gMFI).

959 (E) Il-1α from supernatants of T cells (left) and co-cultured T cells and AMs (right) of
960 young WT (each n=3) and $Terc^{ko/ko}$ mice (each n=3) at 2 and 24 hpi.

961 ns ≥ 0.05, *p < 0.05. P calculated by Kruskal-Wallis-test (D-E). Each replicate is
962 displayed as a data point.

963 **Supplemental Figure 1: Terc$^{ko/ko}$ mice with systemic infection display more**
964 **severe pneumonia with bacteremia and increased mortality.**

965 (A) Clinical score of infected Terc$^{ko/ko}$ mice at the time of infection (0 dpi) and 24 hpi
966 (1 dpi). The mice were divided into three groups according to their clinical score
967 values: mice with mild infection (dark blue dots; n=1), mice with systemic infection
968 (light blue dots; n=2), and mice where infection resulted in a fatal outcome (black
969 dots; n=2). Mice with systemic infection were defined as mice with an increased
970 clinical score and the presence of bacteria in organs other the lung.

971 (B) Bacterial load of kidney and liver tissue of the infected Terc$^{ko/ko}$ mice (each n=3).
972 Light blue data points represent mice with systemic infection, while dark blue dots
973 represent the mouse with mild infection.

974 (C) Bacterial load of the lung of infected mice at 24 hpi. Young WT and old WT mice:
975 n=5; Terc$^{ko/ko}$ mice with systemic infection: n=2, Terc$^{ko/ko}$ mice without systemic
976 infection: n=1. Data is displayed as logarithmic.

977 (D) Relative body weight of young WT (each n=5), old WT (each n=5) and Terc$^{ko/ko}$
978 mice (non-infected: n = 3; with systemic infection: n=2; without systemic infection: n
979 =1). Relative body weight displays body weight at 24 hpi as a percentage of the body
980 weight at the time of infection.

981 (E) Relative lung weight of y young WT (each n=5), old WT (each n=5) and Terc$^{ko/ko}$
982 mice (non-infected: n = 3; with systemic infection: n=2; without systemic infection: n
983 =1). Relative lung weight displays lung weight after 24 hpi as a percentage of the
984 current body weight.

985 (F) Measurement of average telomere length per chromosome end in lungs of young
986 WT (n=4), old WT (n=4) and Terc$^{ko/ko}$ mice.

987 (G) PCA of sequenced lungs from young WT (each n=3), old WT (each n=3) and
988 Terc$^{ko/ko}$ mice (each n=3). The mice with systemic infection clustered separately from
989 the other samples.

990 (H) Number of DEGs per comparison including up- and downregulated DEGs as well
991 as the total count. Differential gene expression analysis was conducted using the
992 DESeq2 software as well as negative binomial distribution. For FDR calculation the
993 Benjamini-Hochberg procedure was used. For each mouse cohort three biological
994 replicates were sequenced and used for analysis.

995 Infected Terc$^{ko/ko}$ mice were divided into systemic and non-systemic infected mice for
996 several analyses (C, D, and E). *$p < 0.05$. P calculated by Kruskal-Wallis-test (C-E).
997 Each replicate is displayed as a data point.

998 **Supplemental Figure 2: Several pathways relevant for inflammation and**
999 **adaptive and innate immune response are differentially expressed in infected**
1000 **Terc$^{ko/ko}$ mice.**

1001 Heatmaps of DEGs related to the NLRP3 inflammasome pathway (A), macrophage
1002 marker (C), Chemokine signaling pathway (D), T helper cell marker (E), or TCR
1003 signaling (F). Red indicates upregulation, and blue indicates downregulation of the
1004 gene. Differential gene expression analysis was conducted using the DESeq2
1005 software as well as negative binomial distribution. For FDR calculation the Benjamini-
1006 Hochberg procedure was used. Heatmaps were constructed using R Studio. Only
1007 significant DEGs (p-value < 0.05) were displayed in the heatmap. Non-significant
1008 genes were set to zero and are shown as white. DEGs are displayed as log2fold-
1009 change. For each mouse cohort three biological replicates were sequenced and used
1010 for analysis. The respective groups used for the comparison are indicated below
1011 each column. All comparisons are shown.

1012 B) Immunofluorescence staining of CD68 (red), actin (purple), and DAPI (blue) of
1013 AMs isolated from Terc$^{ko/ko}$ and young WT mice. Representative pictures are shown
1014 for each group.

1015 **Supplemental Figure 3:**

1016 (A) Gating strategy for the immunophenotyping of cells from murine spleen. First,
1017 lymphocytes were selected, then duplicates and dead cells were excluded (APC-Cy7
1018 negative). To avoid autofluorescence of macrophages, the F4/80 negative population
1019 was selected. For further calculations the CD3^{+} CD19^{-} cell population was used.

1020 (B) Most differentially enriched KEGG pathways of infected Terc$^{ko/ko}$ vs. infected old
1021 WT, infected young WT vs. non-infected young WT and infected Terc$^{ko/ko}$ vs. non-
1022 infected Terc$^{ko/ko}$ mice. The dot plots were constructed using R Studio.

1023 (C) Gating strategy for T cells isolated from murine spleen to asses CD247
1024 expression. First, lymphocytes were selected, duplicates and dead cells were
1025 excluded before selecting CD3^{+} CD247^{+} cells. This population was used for further
1026 calculations.

1027 (D) CD44 expression measured with flow cytometry of non-infected and infected T
1028 cells (left) and co-cultured T cells and AMs (right) of young WT (each n=3) and
1029 Terc$^{ko/ko}$ mice (each n=3) after 24 hpi. CD44 expression is displayed as geometric
1030 mean fluorescence intensity (gMFI).

1031 (E) Heatmap of differentially regulated MSC markers. Red indicates upregulation,
1032 and blue indicates downregulation of the gene. Differential gene expression analysis
1033 was conducted using the DESeq2 software as well as negative binomial distribution.
1034 For FDR calculation the Benjamini-Hochberg procedure was used. Heatmaps were
1035 constructed using R Studio. Only significant DEGs (p-value < 0.05) were displayed in

1036 the heatmap. Non-significant genes were set to zero and are shown as white. DEGs
1037 are displayed as log2fold-change. For each mouse cohort three biological replicates
1038 were sequenced and used for analysis. The respective groups used for the
1039 comparison are indicated below each column.

1040

1041 **Supplemental Figure 4:**

1042 (A) Overview of the methods used in this publication. Illustration was created with
1043 Biorender.

1044

1045 **Supplemental Figure 5:**

1046 (A) Exemplary results of genotyping of $Terc^{ko/ko}$ mice used for breeding. Knockout
1047 mice show a single band at 180 bp, while WT mice have a single band at 200 bp.
1048 Heterozygeous mice (WT/ko) display both bands. Results were analyzed using an
1049 Agilent 2200 TapeStation.

Telomerase RNA component knockout exacerbates *S. aureus* pneumonia by extensive inflammation and dysfunction of T cells

FIGURES

Graphical abstract

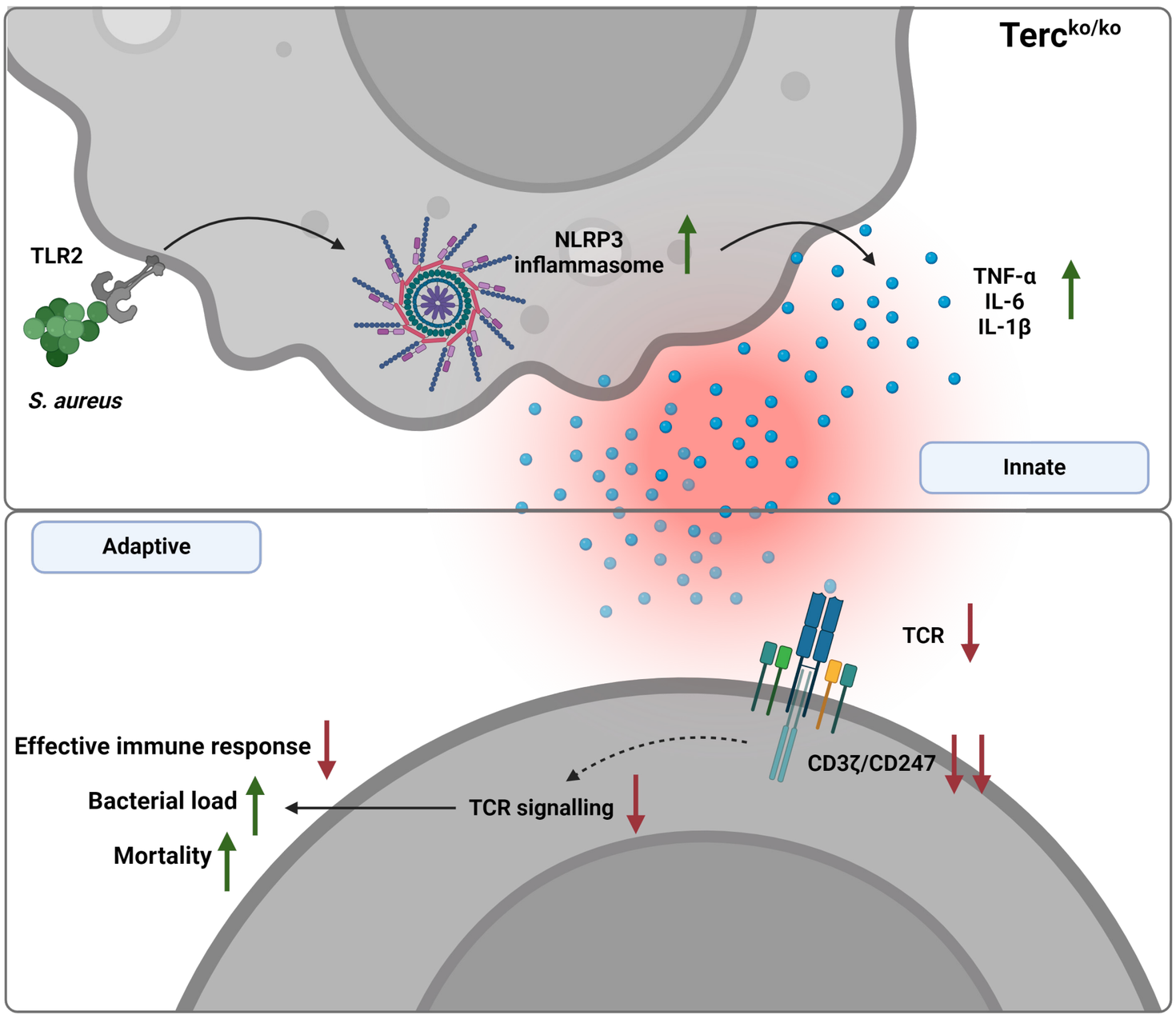

FIGURE 1

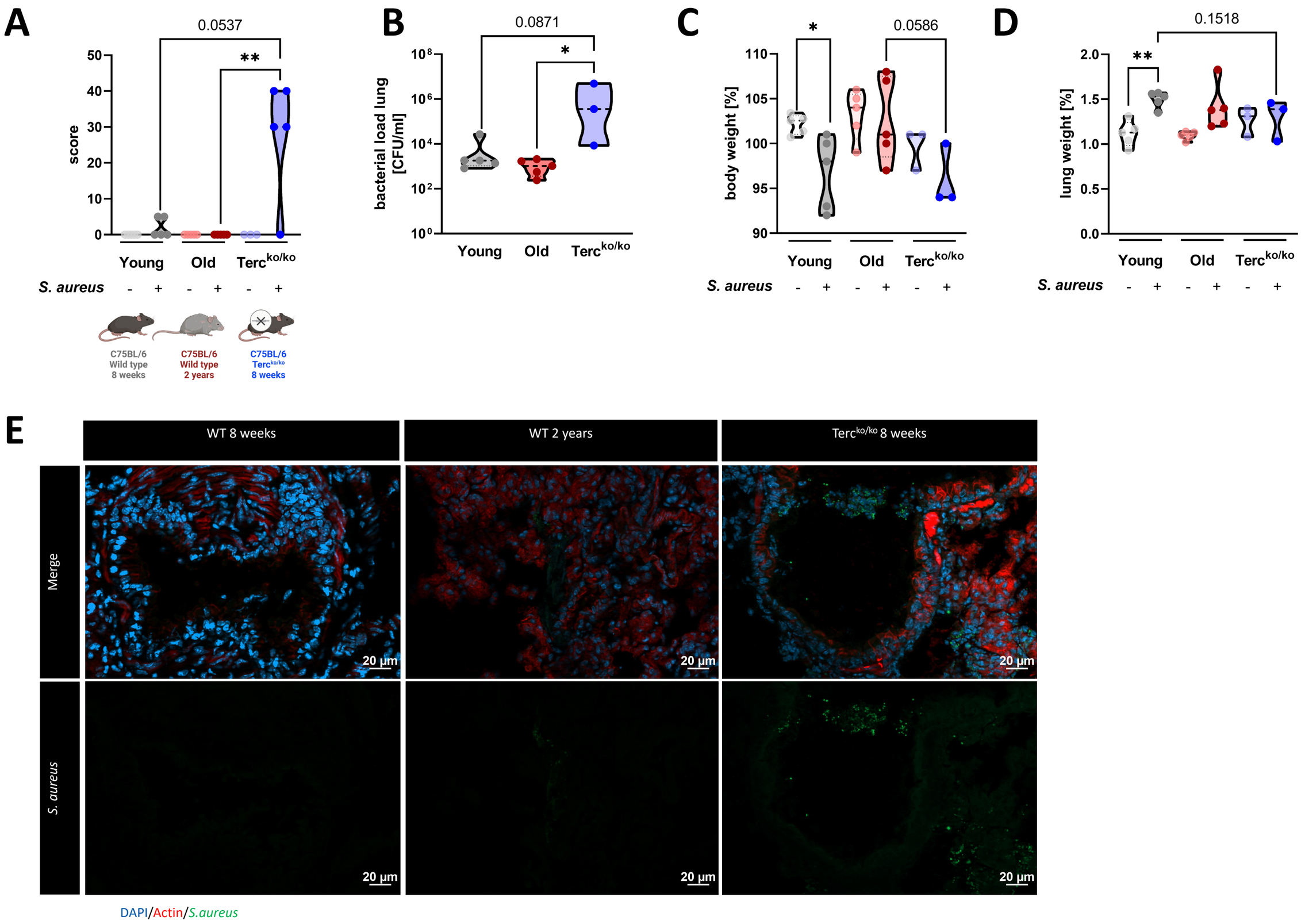
A
0.0537
**
score
Young
Old
Terc ko/ko
S. aureus
C75BL/6 Wild type 8 weeks
C75BL/6 Wild type 2 years
C75BL/6 Terc ko/ko 8 weeks
B
0.0871
*
bacterial load lung [CFU/ml]
C
*
0.0586
body weight [%]
D
0.1518
**
lung weight [%]
E
WT 8 weeks
WT 2 years
Terc ko/ko 8 weeks
Merge
S. aureus
20 µm
DAPI/Actin/S.aureus

FIGURE 2

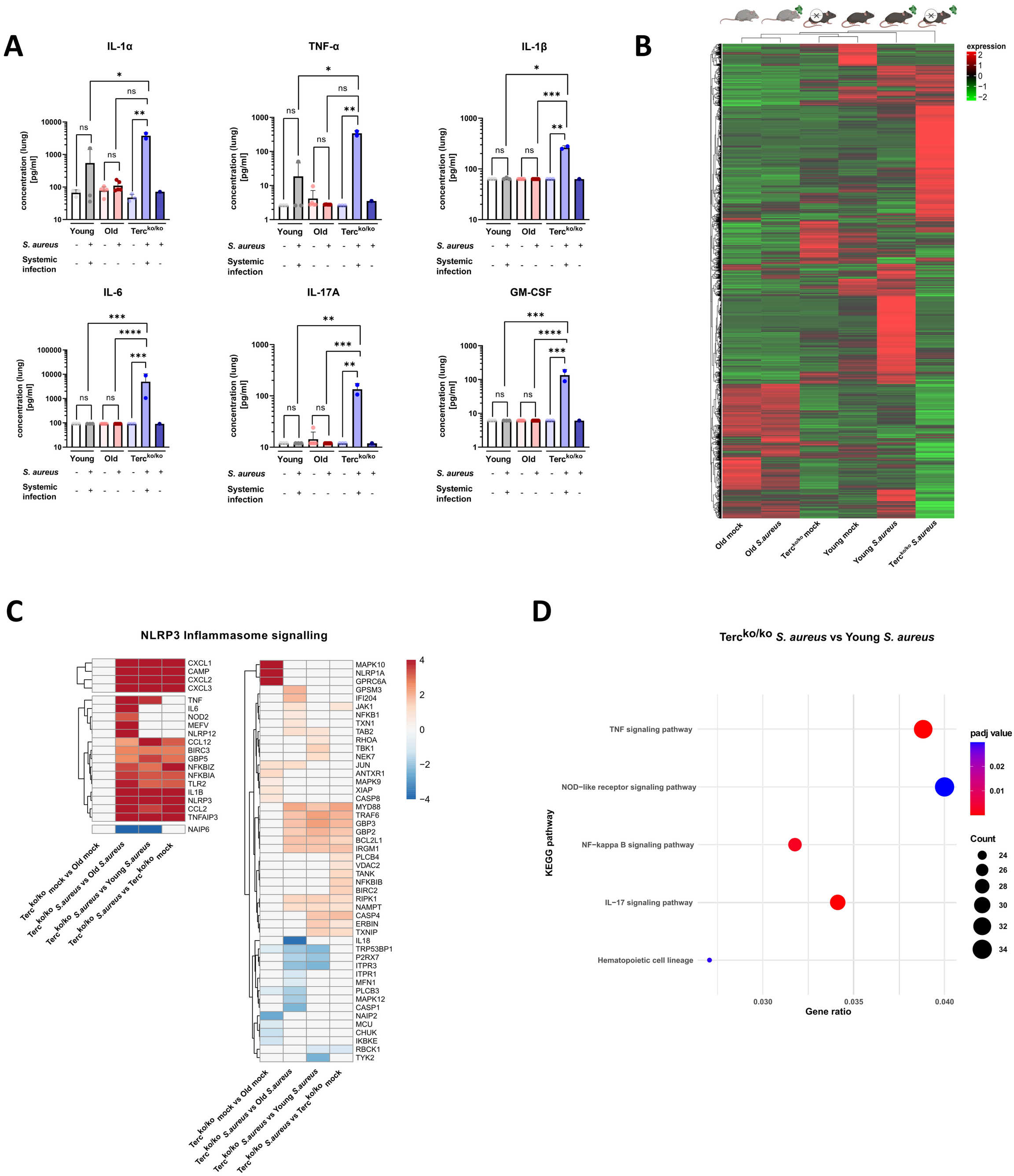
A
IL-1α
TNF-α
IL-1β
IL-6
IL-17A
GM-CSF
concentration (lung) [pg/ml]
Young
Old
Terc ko/ko
S. aureus
Systemic infection
B
expression
Old mock
Old S.aureus
Terc ko/ko mock
Young mock
Young S.aureus
Terc ko/ko S.aureus
C
NLRP3 Inflammasome signalling
CXCL1
CAMP
CXCL2
CXCL3
TNF
IL6
NOD2
MEFV
NLRP12
CCL12
BIRC3
GBP5
NFKBIZ
NFKBIA
TLR2
IL1B
NLRP3
CCL2
TNFAIP3
NAIP6
MAPK10
NLRP1A
GPRC6A
GPSM3
IFI204
JAK1
NFKB1
TXN1
TAB2
RHOA
TBK1
NEK7
JUN
ANTXR1
MAPK9
XIAP
CASP8
MYD88
TRAF6
GBP3
GBP2
BCL2L1
IRGM1
PLCB4
VDAC2
TANK
NFKBIB
BIRC2
RIPK1
NAMPT
CASP4
ERBIN
TXNIP
IL18
TRP53BP1
P2RX7
ITPR3
ITPR1
MFN1
PLCB3
MAPK12
CASP1
NAIP2
MCU
CHUK
IKBKE
RBCK1
TYK2
Terc ko/ko mock vs Old mock
Terc ko/ko S.aureus vs Old S.aureus
Terc ko/ko S.aureus vs Young S.aureus
Terc ko/ko S.aureus vs Terc ko/ko mock
D
Terc ko/ko S. aureus vs Young S. aureus
TNF signaling pathway
NOD−like receptor signaling pathway
NF−kappa B signaling pathway
IL−17 signaling pathway
Hematopoietic cell lineage
KEGG pathway
Gene ratio
padj value
Count

FIGURE 3

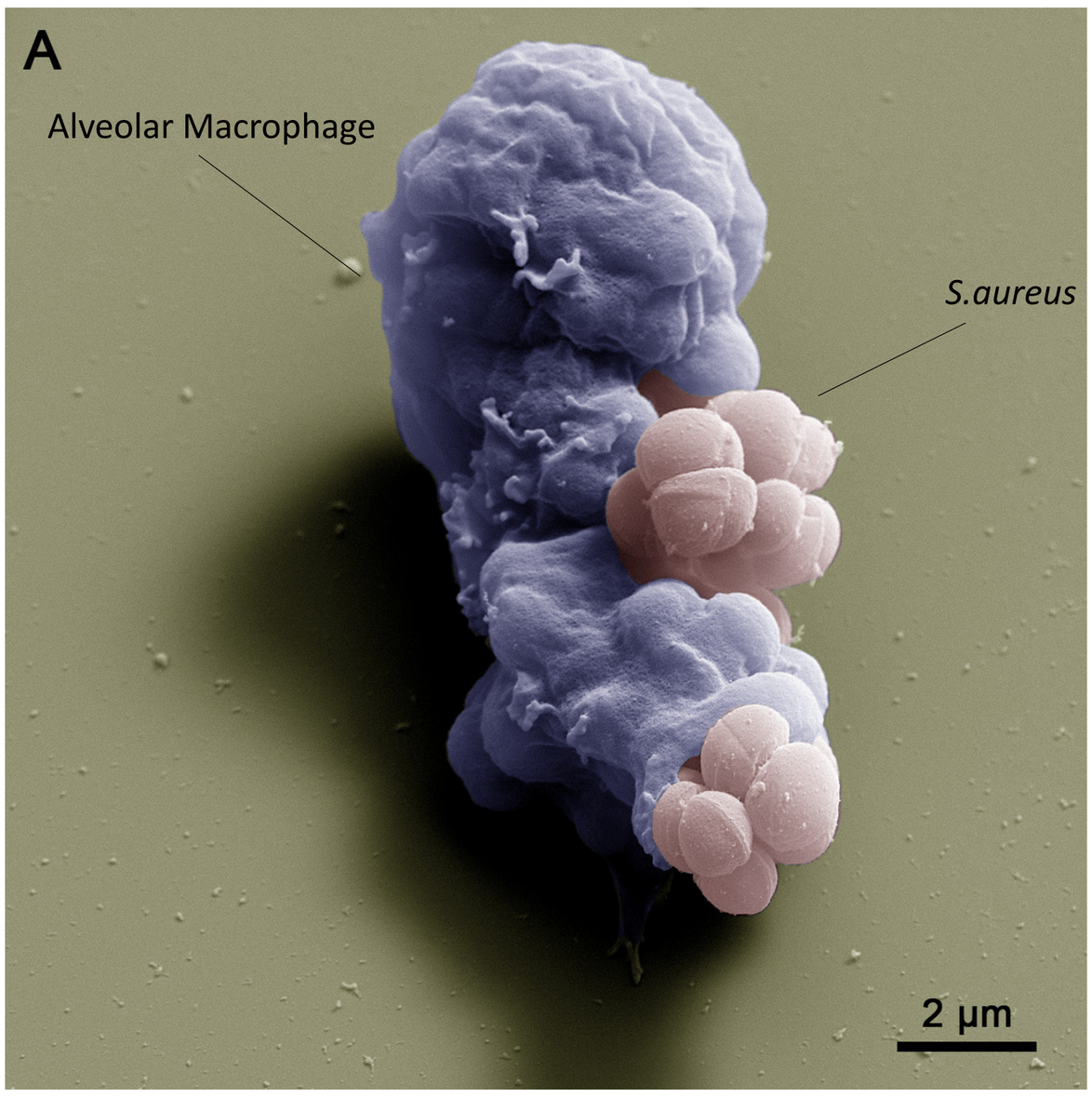
A
Alveolar Macrophage
S.aureus
2 µm

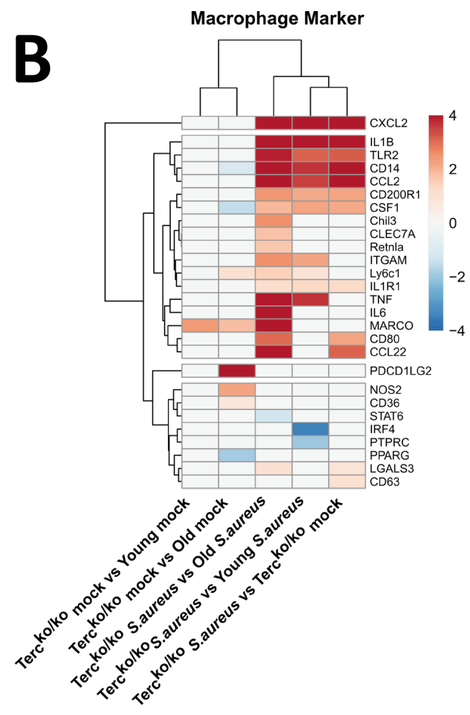
B
Macrophage Marker
CXCL2
IL1B
TLR2
CD14
CCL2
CD200R1
CSF1
Chil3
CLEC7A
Retnla
ITGAM
Ly6c1
IL1R1
TNF
IL6
MARCO
CD80
CCL22
PDCD1LG2
NOS2
CD36
STAT6
IRF4
PTPRC
PPARG
LGALS3
CD63
4
2
0
−2
−4
Terc ko/ko mock vs Young mock
Terc ko/ko mock vs Old mock
Terc ko/ko S.aureus vs Old S.aureus
Terc ko/ko S.aureus vs Young S.aureus
Terc ko/ko S.aureus vs Terc ko/ko mock

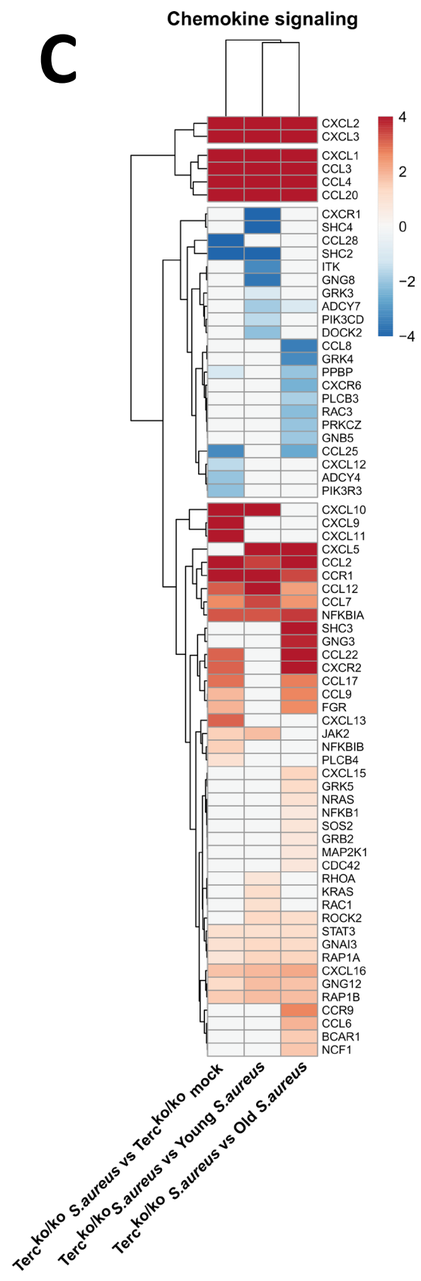
C
Chemokine signaling
CXCL2
CXCL3
CXCL1
CCL3
CCL4
CCL20
CXCR1
SHC4
CCL28
SHC2
ITK
GNG8
GRK3
ADCY7
PIK3CD
DOCK2
CCL8
GRK4
PPBP
CXCR6
PLCB3
RAC3
PRKCZ
GNB5
CCL25
CXCL12
ADCY4
PIK3R3
CXCL10
CXCL9
CXCL11
CXCL5
CCL2
CCR1
CCL12
CCL7
NFKBIA
SHC3
GNG3
CCL22
CXCR2
CCL17
CCL9
FGR
CXCL13
JAK2
NFKBIB
PLCB4
CXCL15
GRK5
NRAS
NFKB1
SOS2
GRB2
MAP2K1
CDC42
RHOA
KRAS
RAC1
ROCK2
STAT3
GNAI3
RAP1A
CXCL16
GNG12
RAP1B
CCR9
CCL6
BCAR1
NCF1
4
2
0
−2
−4
Terc ko/ko S.aureus vs Terc ko/ko mock
Terc ko/ko S.aureus vs Young S.aureus
Terc ko/ko S.aureus vs Old S.aureus

FIGURE 4

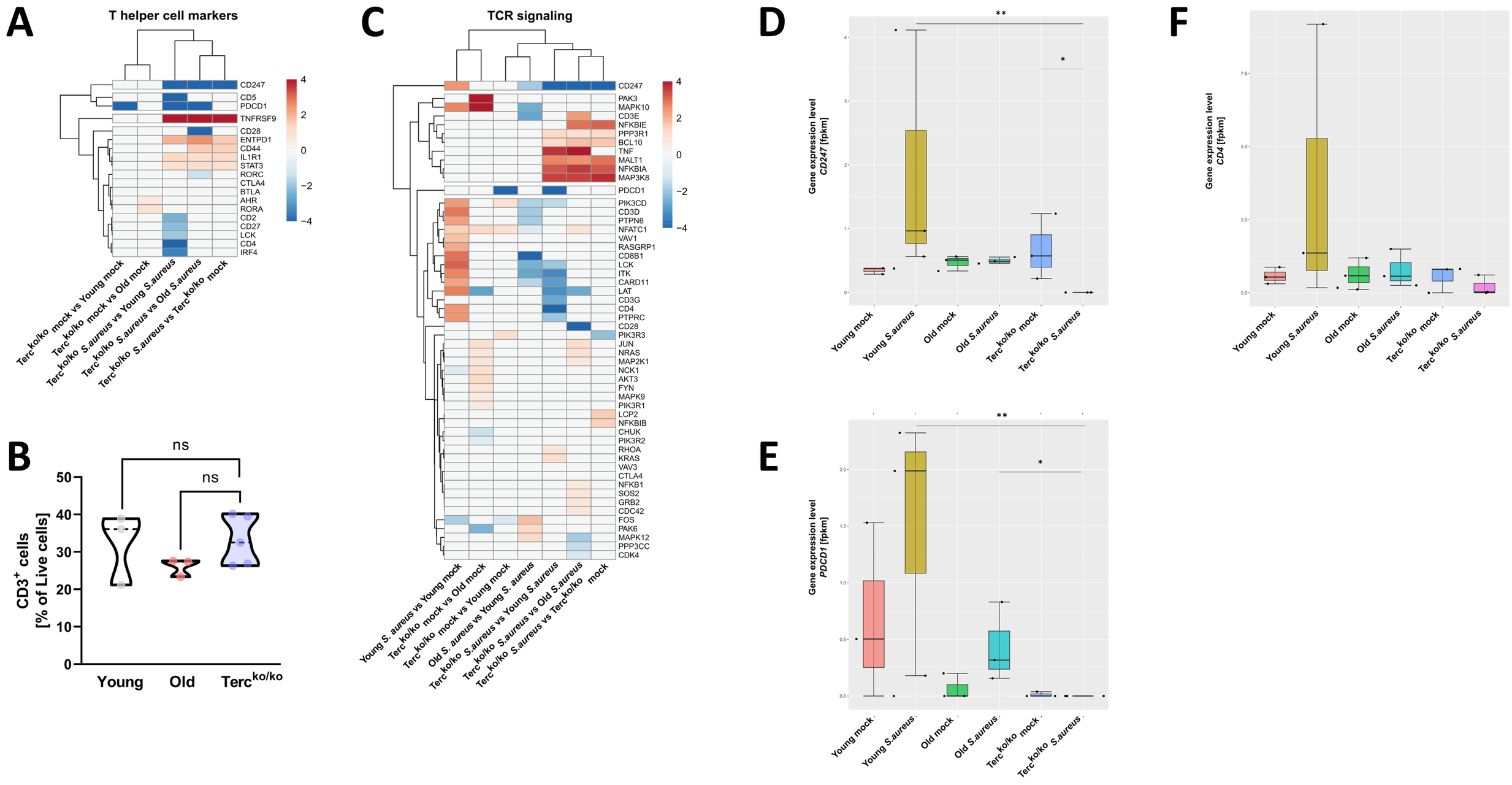
A
T helper cell markers
CD247
CD5
PDCD1
TNFRSF9
CD28
ENTPD1
CD44
IL1R1
STAT3
RORC
CTLA4
BTLA
AHR
RORA
CD2
CD27
LCK
CD4
IRF4
Terc ko/ko mock vs Young mock
Terc ko/ko mock vs Old mock
Terc ko/ko S.aureus vs Young S.aureus
Terc ko/ko S.aureus vs Old S.aureus
Terc ko/ko S.aureus vs Terc ko/ko mock
B
ns
ns
CD3+ cells [% of Live cells]
Young
Old
Terc ko/ko
C
TCR signaling
CD247
PAK3
MAPK10
CD3E
NFKBIE
PPP3R1
BCL10
TNF
MALT1
NFKBIA
MAP3K8
PDCD1
PIK3CD
CD3D
PTPN6
NFATC1
VAV1
RASGRP1
CD8B1
LCK
ITK
CARD11
LAT
CD3G
CD4
PTPRC
CD28
PIK3R3
JUN
NRAS
MAP2K1
NCK1
AKT3
FYN
MAPK9
PIK3R1
LCP2
NFKBIB
CHUK
PIK3R2
RHOA
KRAS
VAV3
CTLA4
NFKB1
SOS2
GRB2
CDC42
FOS
PAK6
MAPK12
PPP3CC
CDK4
Young S. aureus vs Young mock
Terc ko/ko mock vs Old mock
Terc ko/ko mock vs Young mock
Old S. aureus vs Young S. aureus
Terc ko/ko S.aureus vs Young S.aureus
Terc ko/ko S.aureus vs Old S.aureus
Terc ko/ko S.aureus vs Terc ko/ko mock
D
Gene expression level CD247 [fpkm]
Young mock
Young S.aureus
Old mock
Old S.aureus
Terc ko/ko mock
Terc ko/ko S.aureus
E
Gene expression level PDCD1 [fpkm]
Young mock
Young S.aureus
Old mock
Old S.aureus
Terc ko/ko mock
Terc ko/ko S.aureus
F
Gene expression level CD4 [fpkm]
Young mock
Young S.aureus
Old mock
Old S.aureus
Terc ko/ko mock
Terc ko/ko S.aureus

FIGURE 5

A

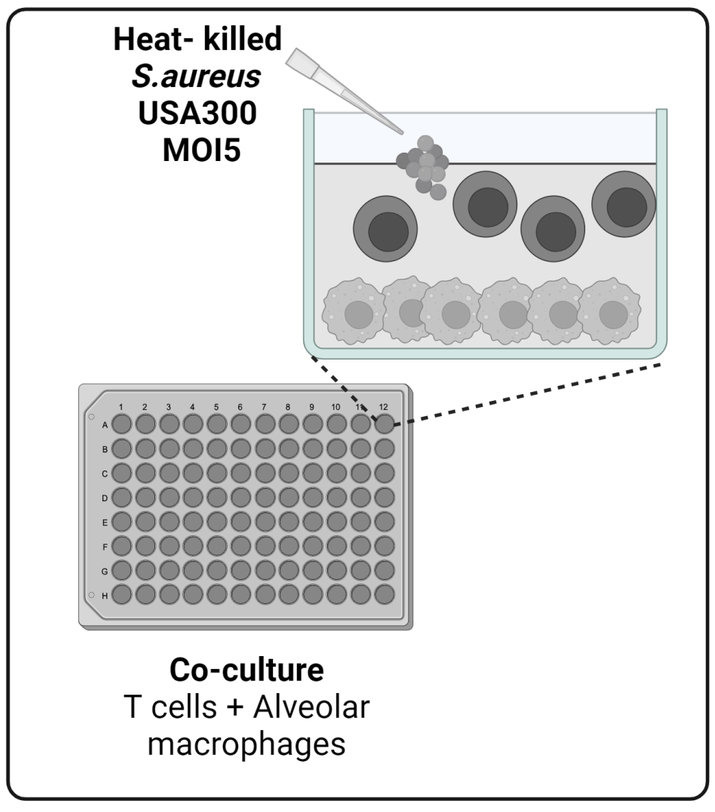

B

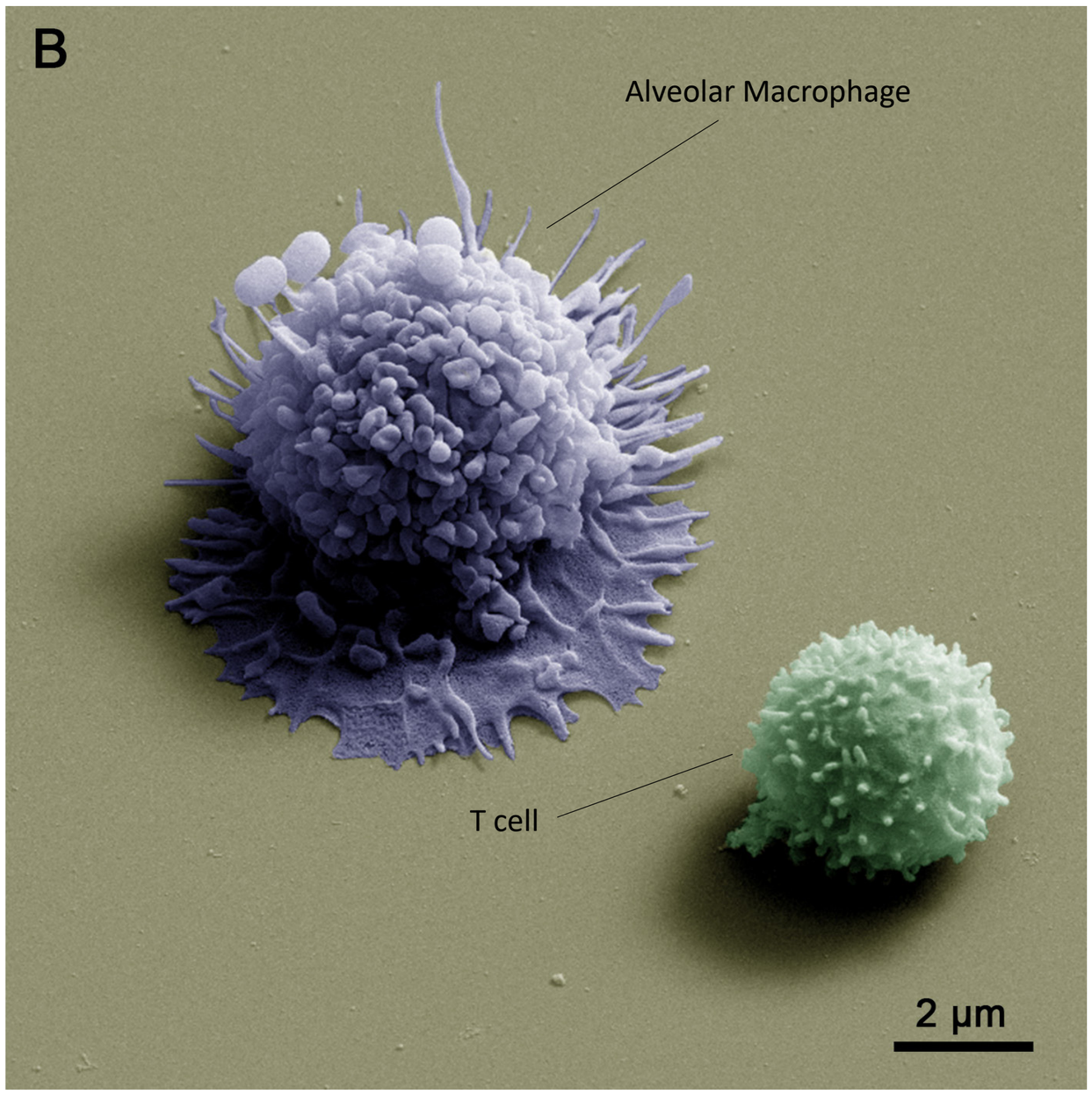

C

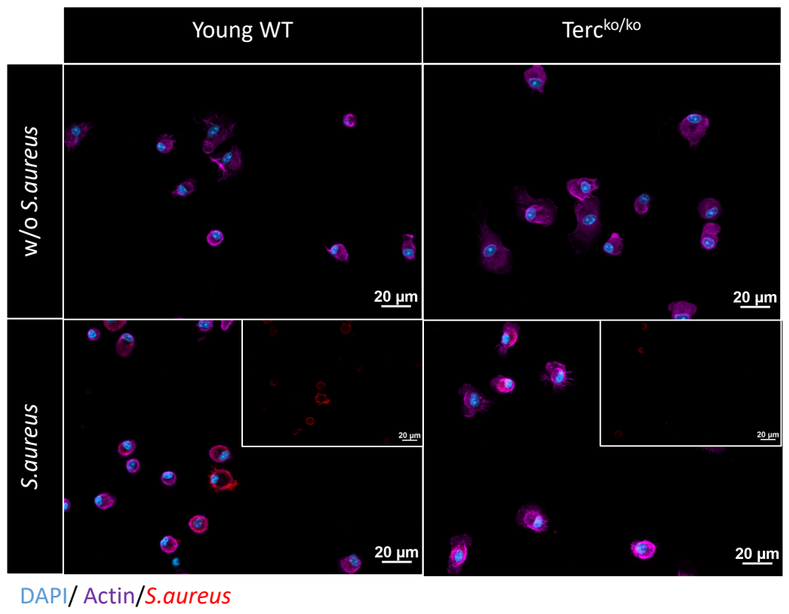

D

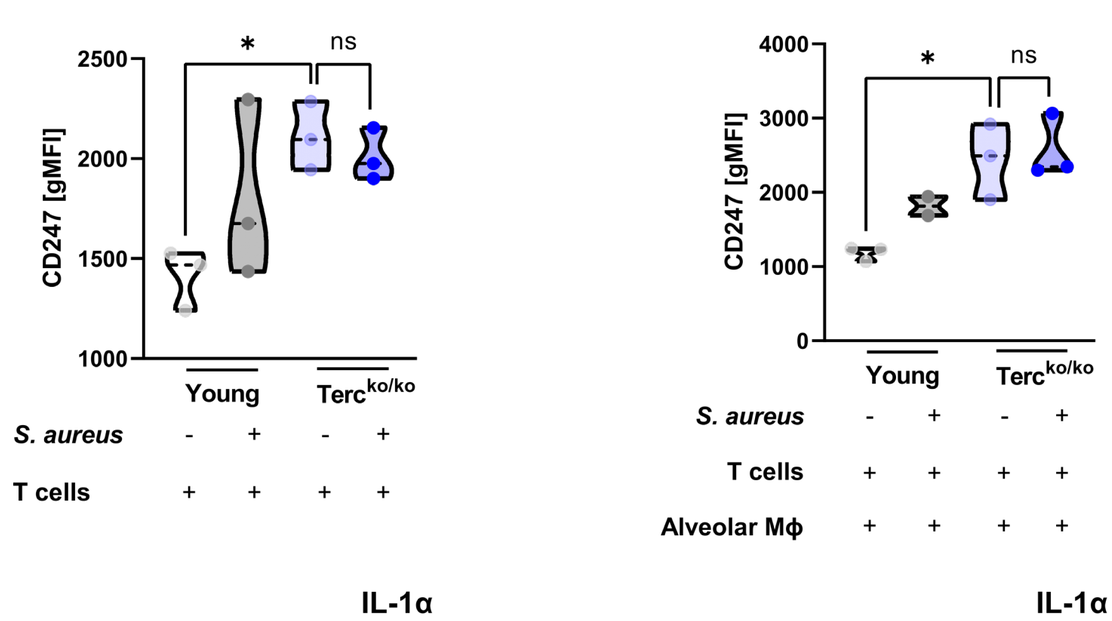
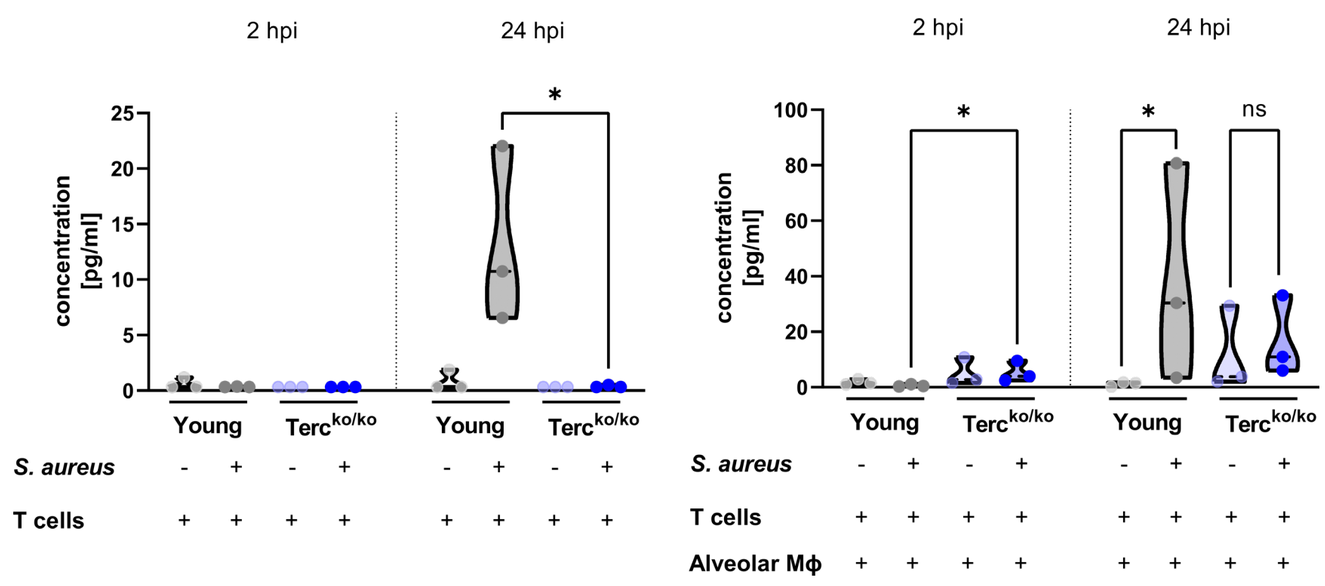
E